ESCAP/WMO
Typhoon Committee

Available online at www.sciencedirect.com

ScienceDirect

Tropical Cyclone Research and Review 12 (2023) 267–293

www.keaipublishing.com/tcrr

Remote sensing and analysis of tropical cyclones: Current and emerging satellite sensors

Lucrezia Ricciardulli [a,*], Brian Howell [b], Christopher R. Jackson [c], Jeff Hawkins [d], Joe Courtney [e], Ad Stoffelen [f], Sebastian Langlade [g], Chris Fogarty [h], Alexis Mouche [i], William Blackwell [j], Thomas Meissner [a], Julian Heming [k], Brett Candy [k], Tony McNally [l], Masahiro Kazumori [m], Chinmay Khadke [n], Maria Ana Glaiza Escullar [o]

[a] *Remote Sensing Systems, Santa Rosa, CA, USA*
[b] *Joint Typhoon Warning Center, Pearl Harbor, Hawaii, USA*
[c] *Global Ocean Associates (supporting NOAA/ NESDIS STAR), Alexandria, VA, USA*
[d] *University of Wisconsin, Cooperative Institute for Meteorological Satellite Studies, Madison, WI, USA*
[e] *Bureau of Meteorology, Perth, Australia*
[f] *Royal Netherlands Meteorological Institute (KNMI), De Bilt, Netherlands*
[g] *Tropical Cyclone/Regional Specialized Meteorological Center, Météo France, Réunion, France*
[h] *Canadian Hurricane Center (CHC), Dartmouth, Nova Scotia, Canada*
[i] *University Brest, CNRS, IRD, Ifremer, Laboratoire d'Océanographie Physique et Spatiale (LOPS), IUEM, Brest, France*
[j] *MIT Lincoln Laboratory, Lexington, MA, USA*
[k] *Met Office, Exeter, UK*
[l] *European Centre for Medium-Range Weather Forecasts, Reading, UK*
[m] *Japan Meteorological Agency (JMA), Tokyo, Japan*
[n] *India Meteorological Department (IMD), New Delhi, India*
[o] *Philippine Atmospheric, Geophysical and Astronomical Services Administration (PAGASA), Diliman Quezon City, Philippines*

Available online 23 December 2023

Abstract

This article describes recent advances in the capability of new satellite sensors for observing Tropical Cyclones (TC) fine structure, wind field, and temporal evolution. The article is based on a World Meteorological Organization (WMO) report prepared for the 10th International Workshop on Tropical Cyclones (IWTC), held in Bali in December 2022, and its objective is to present updates in TC research and operation every four years. Here we focus on updates regarding the most recent space-based TC observations, and we cover new methodologies and techniques using polar orbiting sensors, such as C-band synthetic aperture radars (SARs), L-band and combined C/X-band radiometers, scatterometers, and microwave imagers/sounders. We additionally address progress made with the new generation of geostationary and small satellites, and discuss future sensors planned to be launched in the next years. We then briefly describe some examples on how the newest sensors are used in operations

* Corresponding author. Remote Sensing Systems, 444 10th St, Suite 200, Santa Rosa, CA 95401, USA.
E-mail address: ricciardulli@remss.com (L. Ricciardulli).
Peer review under responsibility of Shanghai Typhoon Institute of China Meteorological Administration.

Production and Hosting by Elsevier on behalf of KeAi

https://doi.org/10.1016/j.tcrr.2023.12.003

and data assimilation for TC forecasting and research, and conclude the article with a discussion on the remaining challenges of TC space-based observations and possible ways to address them in the near future.

Keywords: Tropical cyclones; Surface wind; Satellite sensors; Operations

1. Introduction

In-situ monitoring of tropical cyclone (TC) formation and evolution is limited to small geographic regions. The data sparsity in the tropical oceanic domains at the global scale necessitates satellite remote sensing be the primary tool for monitoring TC location, structure, and intensity in near real-time (NRT). These satellites occupy both geostationary (GEO) and low earth orbit (LEO) and include sensors using visible and infrared (VIS/IR), passive microwave (PMW), and active microwave (scatterometers) frequencies. Recent advances in space-based observations of TCs were presented at the World Meteorological Organization (WMO) 10th International Workshop on Tropical Cyclones (IWTC), held in Bali in December 2022 (WMO, 2022), and are summarized in this paper. Building on a previous WMO report in the context of the 9th International Workshop on Tropical Cyclones (WMO, 2018), we discuss the recent developments in the past four years regarding new and emerging satellite sensors (Section 2), their advantages and limitations, and how they have been used by the operational community. The storms properties and geophysical variables of high interest for TC monitoring and forecast are: frequent observations of the exact location of the storm's center, the eye's width, the intensity, the extent of the region affected by gale, storm and hurricane force winds, temperature and moisture distribution, precipitation rate and convective features, and any rapid change to the storm intensity or structure (e.g. rapid intensification, eye replacement cycles). The list of newer satellite sensors starts with the Synthetic Aperture Radar (Section 2.1) which brought significant advancements in the capability of observing fine details of the storms' core from space. The other categories of remote sensors discussed here are: L-band radiometers including SMAP/SMOS (2.2), combined C/X-band radiometers such as AMSR2 (2.3), C- and Ku-band scatterometers (2.4), Microwave Imagers/Sounders (2.5), Geostationary satellite sensors (2.6), the Doppler Lidar Wind profiler Aeolus (2.7), the GNSS Reflectometer mission CYGNSS (2.8), and SmallSats (e.g., COWVR) and CubeSats (e.g., TROPICS, TEMPEST) (2.9). The following sections present a brief update on recent advances in operations (Section 3) and in data assimilation (4), and a list of planned sensors (5). The manuscript ends with a summary and a list of current challenges faced by the TC observational and operational community (Section 6). Additional details are provided in the following appendices: An acronym list (Appendix A); a table summarizing satellite sensors characteristics (Appendix B); data distribution links (Appendix C), and a list of the data sources used by some operational centers (Appendix D).

2. Current sensors

2.1. SAR

Satellite-based Synthetic Aperture Radars (SARs) have become an important source of information on tropical cyclones due to their unique ability to directly observe the ocean surface with very high resolution (<100 m, when in wide-swath mode, which is typically used for TCs). SAR works by transmitting C-band microwave radar pulses and recording both the amplitude and phase of the reflected return signals (Martin, 2014). These return pulses are then coherently combined over a specific time interval to produce a high resolution 2D image of radar backscatter. SAR wind products are averaged at 3 km resolution. It has been shown that the SAR backscattered signal for cross-polarized channels retains good sensitivity even at very high winds and in rainy environments (Mouche et al., 2017, 2019; Zhang and Perrie, 2012). These features, combined with the high spatial resolution, allow the determination of important storm parameters (e.g. the maximum wind speed, the radius of maximum winds and the distance and areal extent of winds at the critical wind speed thresholds of 34, 50, and 64 knots, identified as R34, R50, and R64, respectively) (Knaff et al., 2021). The SAR imagery has unique capability in viewing the core of the storm, and directly captures many of the well-known tropical storm features such as the eyewall, meso-vortices (circulations within the eyewall), boundary layer rolls, outflow boundaries, and rainbands. These promising capabilities emerged at the IWTC-9 in 2018 (WMO, 2018) as these data were then becoming more accessible to forecasters. Unlike scatterometers and radiometers, due to the high resolution (and high data volume) of the SAR imagery only a portion (~30 %) of every orbit can be collected and downloaded, and the selection must be programmed in advance which limits its TC collection opportunities. The need for additional SAR TCs acquisitions led to a WMO request to the European Union's Earth Observation Programme (the space component of Copernicus) to prioritize access to SAR data collection from Sentinel -1A and 1B satellites in wide swath mode (400 km) over global tropical cyclones.

Much progress has been made since then, resulting in a preliminary internationally coordinated framework for processing SAR TC acquisitions into a wind product, and disseminating them to the operational community in NRT,

addressing one of the actionable recommendations from the WMO IWTC-9 meeting. The latency of the SAR products has also improved in the last two years, fulfilling the operational requirements (<6 h) more than 90 % of the time.

Currently, four SAR missions are being used to study and monitor tropical cyclones: 1) Sentinel-1, a two-satellite system (1A and 1B), developed and operated under the European Space Agency's (ESA) Copernicus Earth Observation Program; Note that Sentinel-1B mission ended due to an anomaly after December 2021; 1A is still operating. 2) The Canadian Radarsat-2, owned and operated by MDA Space. Researchers at NOAA's Center for Satellite Applications and Research's (STAR) and the French Institute for Ocean Science (Ifremer) have been working together to plan and acquire the SAR coverage for the Sentinel and Radarsat missions over tropical cyclones to support operational forecasters at the Joint Typhoon Warning Center (JTWC) and the National Hurricane Center (NHC) (Jackson et al., 2021). From 2019 through 2022 Sentinel-1 and Radarsat-2 acquired imagery on 156 tropical cyclones (worldwide). Fig. 1 is an example of an ocean surface wind speed map and radial wind profile derived from the Sentinel-1 SAR collection over TC Halima (SH22) on 24 March 2022. The active collection planning at STAR and Ifremer is ongoing. 3) The third system is the Radarsat Constellation Mission (RCM), a three-satellite system developed and operated by the Canadian Space Agency that recently begun to support Tropical Cyclone collections. In 2022, the Canadian Space Agency as part of its Hurricane Watch program improved its RCM TC acquisition planning process to provide more TC collections with a corresponding increase in the percentage number of "eye hits". As a result, in 2023 (through 1 June) RCM has provided coverage on 14 named TC systems covering the storm center in more than 75 % of its 105 collections. RCM provided unpresented coverage of TC Freddy collecting 44 images over a 32-day period.

4) The fourth currently operating SAR mission is Gaofen-3 (GF-3), launched in 2016. This is the first Chinese space-borne multi-polarization synthetic aperture radar (SAR) installed at C-band. It collects the data of VH polarized wide ScanSAR (WSC) (Li et al., 2018). Fig. 2 illustrates the retrieved fine ocean surface wind field of Super Typhoon LEKIMA (2019) with 100m horizontal resolution from GF-3 (Fang et al., 2022). This SAR data is not available to the international operational community.

It is worth noting that the Japanese space agency (JAXA) and Meteorological Research Institute (MRI) organized a dedicated Tropical Cyclone campaign to get acquisitions from the Japan L-Band SAR PALSAR-2 over hurricanes. These data were used to develop an algorithm and provide wind speed estimate at 3-km resolution (Isoguchi et al., 2021) and demonstrated the potential for the joint use of L- and C-band SAR sensors.

The opportunities for SAR TC coverage are expected to expand through additional observations from Sentinel-1C (as replacement for 1B) scheduled for launch in 2023 and NASA's NISAR (NASA–Indian Space Research Organization SAR Mission) mission due to launch in 2024, which includes L- and S-band SARs.

2.2. L-band radiometers: SMAP/SMOS

Observations of TCs from L-Band radiometers SMOS (Ifremer), (Reul et al., 2012; 2016) and SMAP (Remote Sensing Systems, REMSS) (Meissner et al., 2017) were emerging at the IWTC-9 (WMO, 2018). Similar to SAR, these sensors do not lose sensitivity at extreme winds and are mostly unaffected by rain, allowing wind observations of up to 70 m/s. However, the L-band radiometers have lower spatial resolutions (40 and 50 km, for SMAP and SMOS, respectively), and are not able to resolve fine structure features visible with the

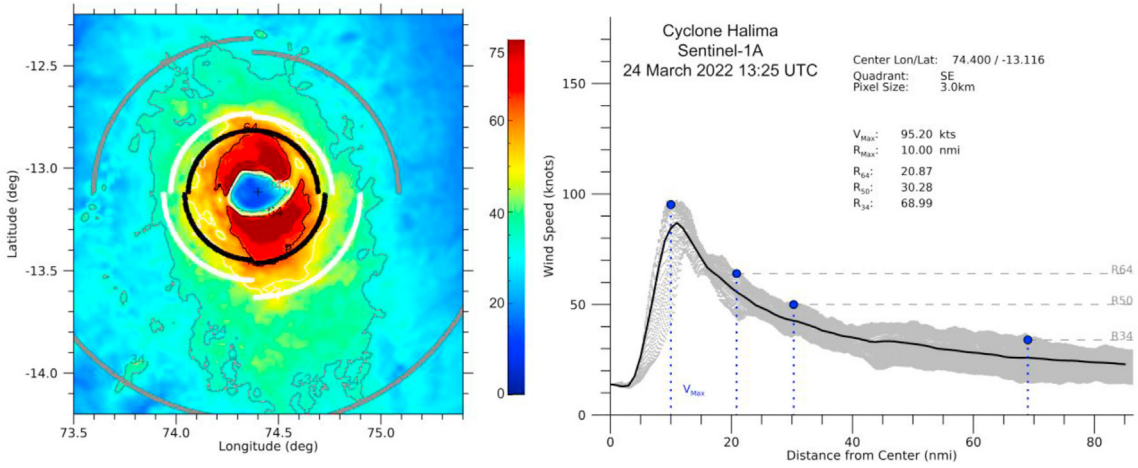

Fig. 1. SAR-derived wind speed map (left) for Cyclone Halima on 24 March 2022 from Sentinel-1A, from the NOAA SAROPS webpage (appendix C). The black, white and grey curves represent the derived fixes for the storm. Wind speed profiles (right) for the Southeast quadrant. Grey dots represent SAR-derived 3 × 3 km wind speeds in the quadrant and the solid back line represents the average wind speed at each distance from the storm's center. The blue dots are the radii of the (64/50/34 kt) fixes along the radial profile and correspond to the quarter circle locations shown in the left-hand plot. They are located at the 95 % percentile of the particular fixes wind speed.

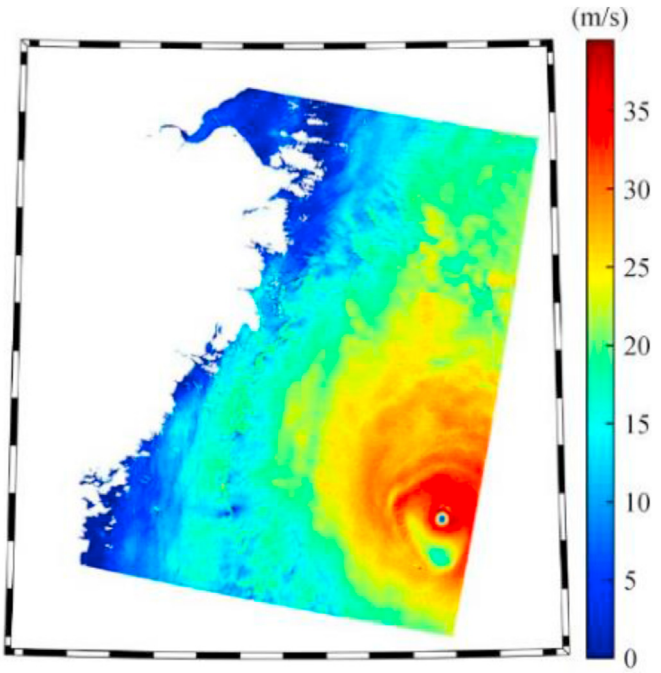

Fig. 2. Wind speed retrieved from the GF-3 SAR image for Lekima (WP10) at 21:56 UTC on 8 August 2019. Max intensity is 38.9 m/s. The displayed longitude/latitude range is (119-125E; 25–31N). Image from (Fang et al., 2022).

SAR, like wind gradients in the core of the storm, or detect the location of the eye in very small storms. The advantage over the SAR is that SMAP and SMOS have a very wide swath (~1000 km), and the acquisition is continuous (14 orbits/day), often providing a daily view of a storm. They also provide consistent measurements over time, and allow for the detection of rapid intensification events. The most common use of these of measurements is the automated production of TC fixes in near real time (NRT, ~3 h), for each named storm in all basins; gridded daily maps are also distributed to the public in NRT. The TC fixes are simple text files that include accurate estimates of the radii for gale, storm and hurricane-force winds for each of the storm quadrants, and an estimate of the 10-min maximum sustained wind (see example of satellite-derived radii in Fig. 3). While emerging at the last IWTC-9 meeting, these fixes are now also routinely distributed via the US Navy Automated Tropical Cyclone Forecast (ATCF) system (Sampson and Schrader, 2000) (link in Appendix C) and used in some operational centers, such as the JTWC (Howell et al., 2022) (see also table in Appendix D). Early validation of these data in TCs used the airborne Stepped Frequency Microwave Radiometers (SFMRs) (Meissner et al., 2017; Reul et al., 2016).

More recently, significant efforts validating the SMAP/SMOS versus SAR were pursued at Ifremer (Zhao et al., 2018), and are available on https://cyclobs.ifremer.fr/app/comparison/stats. In the wind speed range 10–50 m/s, L-band radiometers are very consistent with the SAR (Fig. 4). Above 50 m/s, there is a tendency for the L-band radiometers to have higher winds speeds than SAR. These could be due to impact of rain or waves, improper calibration of the wind retrieval models at these extreme wind regimes, which could affect any of these sensors, or inaccuracies in the SAR wind retrievals at extreme observational incidence angles. Additional discrepancies might result from incorrect methodology used when comparing wind observations from sensors at very different spatial resolutions such as from SAR and L-band radiometers, which requires a resampling of the high-resolution dataset on the same grid of the low resolution one. (Manaster et al., 2021; Meissner et al., 2017) describe some gaussian-weighted resampling methodologies applied when comparing SFMR, or the HWRF high resolution model winds to SMAP and AMSR2. A more in-depth investigation about the inconsistencies between SAR and L-band radiometers at wind speeds above 50 m/s is desirable. Despite some shortcoming, L-band radiometers have been proven useful in remote regions, especially in the Pacific/Indian basins where no air reconnaissance is available. Notice that SMAP suffered a hardware failure on Aug 8, 2022, but it has been restored to NRT operation in October 2022.

2.3. C/X-band radiometers: AMSR2 TC-winds

New TC-dedicated algorithms from C-X band radiometers such as AMSR-2 were developed in 2021 at REMSS. Unlike traditional global all-weather wind algorithms, these new TC-winds are specifically trained for TCs. They were developed initially for WindSat and later for the AMSR sensors, using SMAP winds for training an algorithm that uses a combination of C and X-band channels to remove the effects of rain in storms (Meissner et al., 2021). The TC-winds have been validated compared to HWRF winds (Manaster et al., 2021), and they display similar performance as SMAP: low resolution, but high sensitivity at extreme winds. Gridded maps and fixes are available in NRT and archived back to 2012 (for AMSR2) and 2002 (AMSR-E), for research purposes. The consistency between the intensity estimated from SMAP and AMSR2 TC-winds is illustrated in an example for TC Freddy (Fig. 5). In the absence of SMAP, the AMSR2 TC-winds can be considered their replacement, although some residual rain impact affects the AMSR2 wind retrievals at intense rain rates and winds below hurricane-force. This impact is currently under investigation, and might result in future updates to the AMSR2 all-weather and TC-wind algorithm. The same TC-algorithm can be used in the future AMSR3 radiometer, planned for mid-2024 to early 2025. Similarly, the TC-winds have been processed for the WindSat radiometer and are archived for the period 2003–2020. Global all-weather AMSR2 winds are also produced by REMSS, by NOAA (Alsweiss et al., 2021) and by JAXA (Shibata, 2006). From these radiometers, the rain field and water vapor retrievals could be useful for TC structure, but are not used yet in operations.

2.4. Scatterometers

Scatterometer ocean surface vector winds (OSVW) have been continuously available since 1992 at C-band (e.g., ERS, ASCAT) and Ku-band (e.g., QuikSCAT, RapidScat, ScatSat):

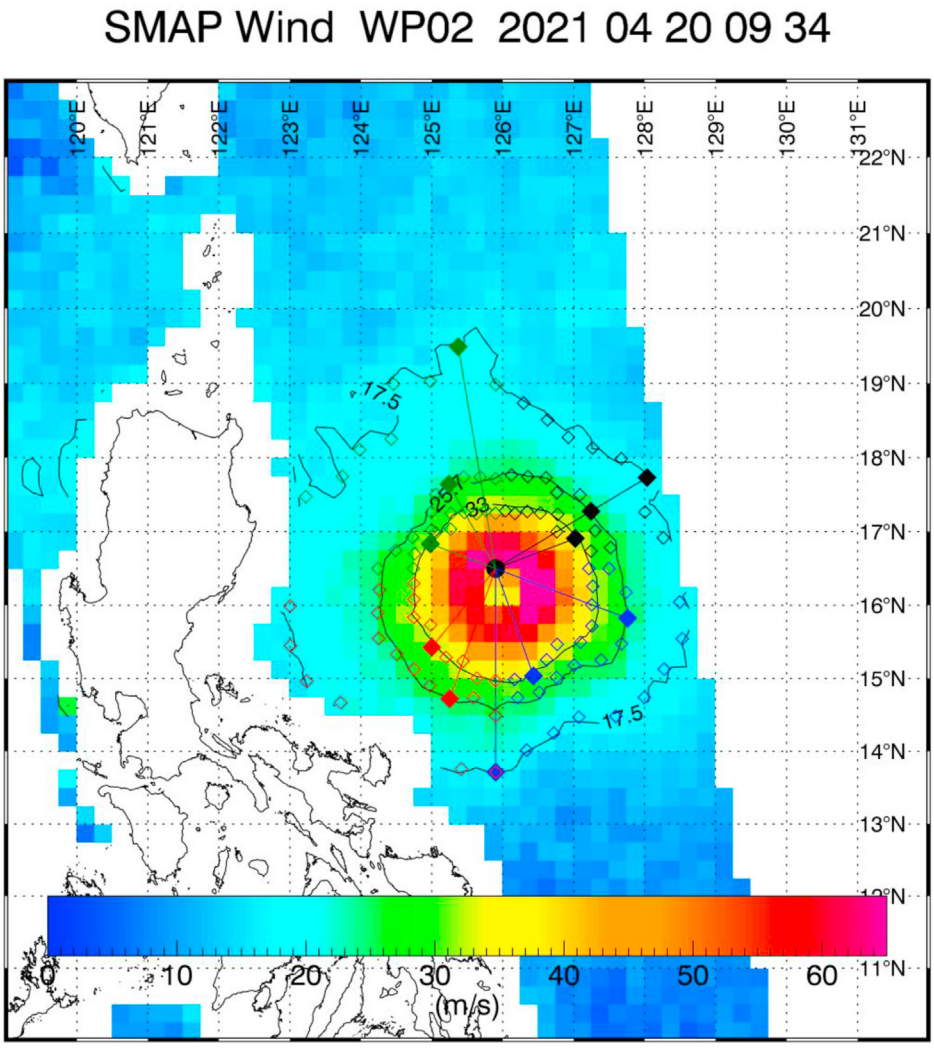

Fig. 3. Automated SMAP fix image for TC Surigae (2021). Radii for gale, storm and hurricane force winds are determined in NRT from the storm center interpolated from the 6-hourly Best-Track storm centers (large filled black circle). The unfilled diamond-shaped symbols refer to the radii of 35/50/64 kt (17.5/25/33 m/s contour lines) for each 10 degrees of azimuthal angle, starting from the storm center. The 80 % percentile of these radii represent the final estimate in each quadrant (filled diamond-shaped symbols), and are distributed to the operational centers via a TC-fix text file (see Appendix C).

in the context of TCs, they are used for operational purposes and to determine trends in extreme winds in thematic Climate Data Records (CDR) (Wentz et al., 2017). A particular asset of scatterometry lies in the spatial extent of the swath (~1000 km), providing OSVW sampling that is sufficient to capture most TCs in several stages of their development. The long tradition of scatterometers in TC operations continues with the C-band European EUMETSAT MetOp ASCAT-B and most recently ASCAT-C (2018) (ASCAT-A was decommissioned in November 2021). These are processed and distributed in NRT by KNMI/OSI SAF (see example in Fig. 6) (Stoffelen et al., 2017b) and by NOAA (Soisuvarn et al., 2013), using different algorithms. The NOAA ASCATs have been calibrated at high winds using in-situ air recon observations. It has been reported that the KNMI ASCATs tend to underestimate high winds, and operational centers using this specific source of ASCAT data are advised to apply a high wind (>12 m/s) scaling correction suggested at the IWSATC-3 meeting in 2021 (Polverari et al., 2022; WMOIWSATC-3, 2022). REMSS also processes ASCAT winds but, at this time, with a latency of few days as a CDR product: the REMSS ASCAT winds are cross-calibrated at all wind speeds with all their active/passive MW sensors, and useful for research (Ricciardulli and Manaster, 2021). Operational Ku-band scatterometer winds are based on the heritage of NASA missions (NSCAT, SeaWinds, and QuikSCAT): they are currently delivered by the Chinese NSOAS HY2A scatterometers (HSCAT-B, -C and-D) (Wang et al., 2020; 2021). The Indian (ISRO) Ku-band scatterometer ScatSat mission ended in February 2021. A follow-up scatterometer mission ISRO OceanSat-3 OSCAT has been recently launched in November 2022, but the data is not operational yet (see Section 5.1).

The scatterometers observe the wind vector with a typical resolution of 12.5–50 km. The wind speeds are significantly attenuated by rain at Ku-band (Ricciardulli and Wentz, 2015; Stiles and Yueh, 2002; Xu and Stoffelen, 2020), but are less

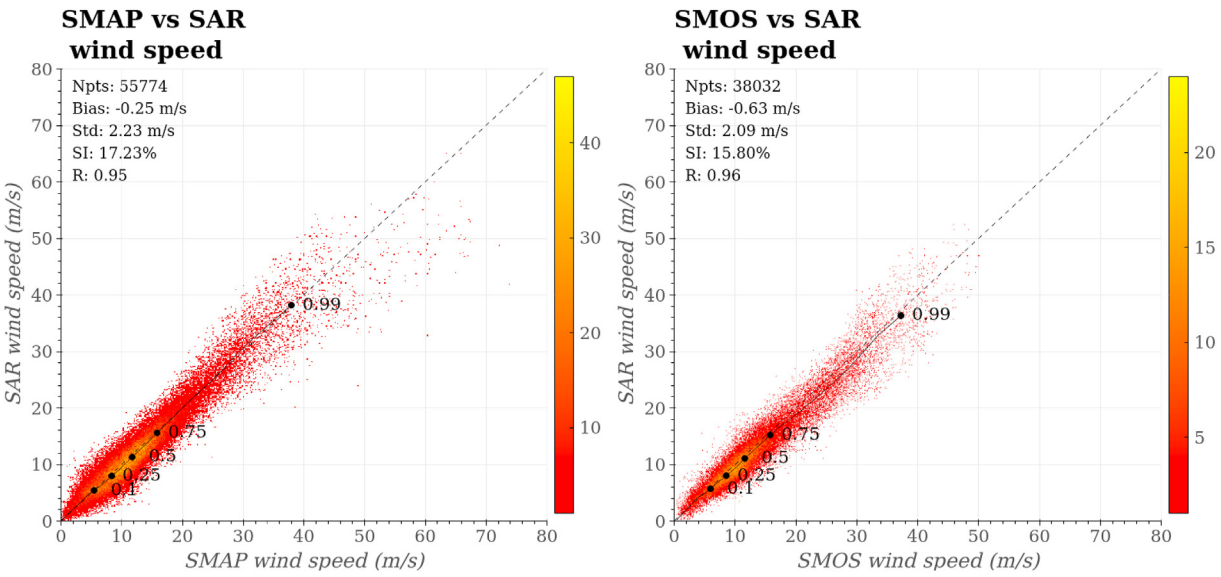

Fig. 4. Statistics of SAR collocations with SMAP (left) and SMOS (right) collected over more than 100 acquisition for each comparison. The statistics include the number of collocations, bias and standard deviation, correlation coefficient and the scatter index SI, defined as the ratio of the RMSE and the average SAR wind speed. The black line is the quantile-quantile line, with some reference values highlighted with black dots. (See https://cyclobs.ifremer.fr/app/comparison/stats for updated SAR vs SMAP/SMOS statistics).

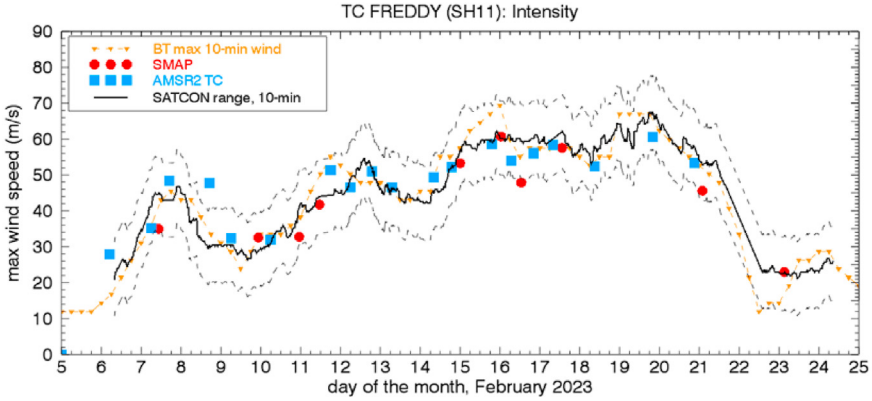

Fig. 5. Timeseries of the intensity (maximum 10-min sustained wind) from the SMAP (red) and AMSR2 (blue) TC-winds during the Southern Hemisphere TC Freddy (SH11) over the month of February 2023. Only satellite passes with a very good coverage of the TC core are displayed here. Also displayed are the intensities from the Best-Track data (orange, https://www.metoc.navy.mil/jtwc/jtwc.html?best-tracks) and from the satellite consensus product SatCon (black, https://tropic.ssec.wisc.edu/real-time/satcon/), which includes an uncertainty range (dashed black lines), both scaled from 1-min to 10-min sustained winds for comparison with the satellite intensities.

affected at C-band (Portabella et al., 2012; Ricciardulli and Manaster, 2021). C-band co-polarized scatterometers such as ASCAT suffer from a reduced sensitivity/saturation at very high winds, which can result in underestimated ASCAT wind speeds above 35–40 m/s. A similar limitation is found in the VV-pol SAR channels (Mouche et al., 2017). The polar orbiting scatterometers are heavily used by forecasters for the analysis of tropical cyclone location, intensity, radial and rotational structure, and identification of the storm center. Most of these scatterometers are on sun-synchronous satellites and cover 6:00/18:00 (HY2B), 9:30/21:30 (ASCATs) and 12:00/00:00 (ISRO scatterometers OSCAT, which ended in Feb 2021; or OceanSat-3, launched in Fall 2022) Local Solar Time (LST) (see table in Appendix B). In addition, HSCAT-C and HSCAT-D are in complementary non-sun-synchronous orbits and hence deliver winds at another four times a day, which vary with time. Hence, over certain periods, scatterometer winds are available every 3 h. It is of great relevance to the global scatterometer wind users to obtain these operational winds in a timely fashion and at a homogeneous service level. This is the aim of the EUMETSAT Ocean and Sea Ice Satellite Application Facility (OSI SAF).

A new topic for scatterometer winds in tropical hurricanes is spatial resolution enhancement. This is being addressed by the past ESA Satellite Hurricane Observation Campaigns (SHOC) and the ongoing Cyclone Monitoring Service (https://

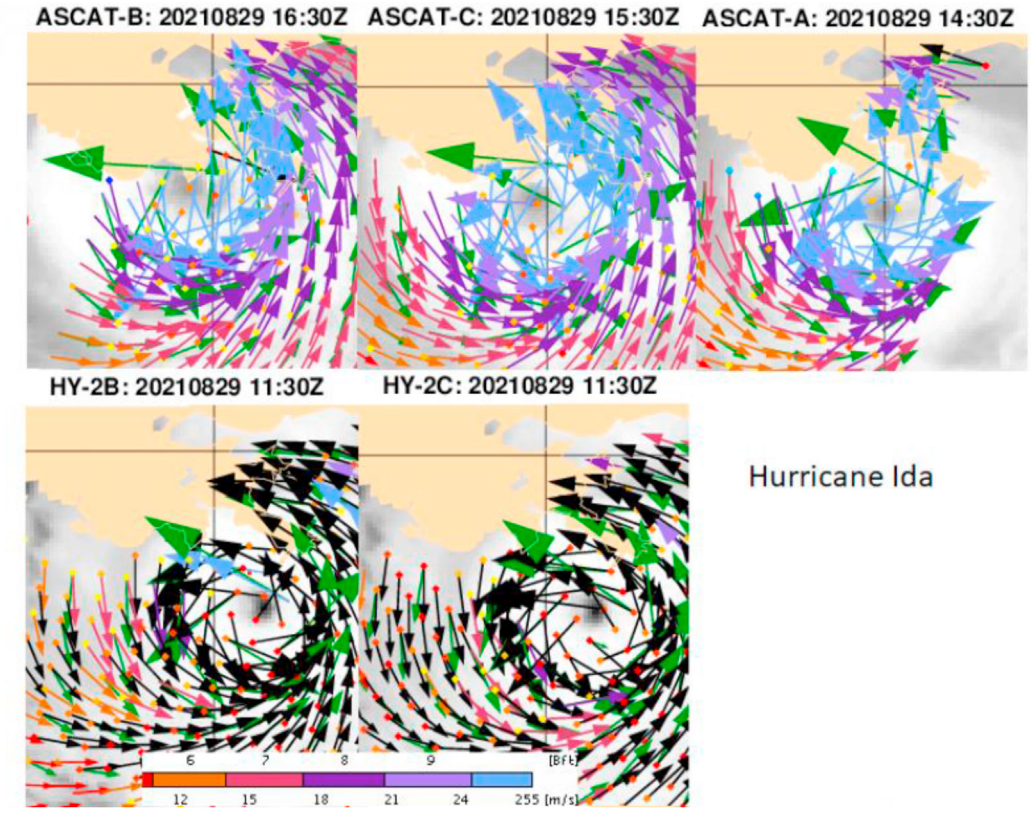

Fig. 6. KNMI/OSISAF ASCAT-A, -B, and -C, HY-2B and -2C views over the same domain for Hurricane Ida (2021) before landfall in Louisiana (near 270E, 29N). Scatterometer vector winds are illustrated with a background GEO infrared satellite image and ECMWF winds in green, valid at the time of observation. The scatterometer winds are colored according to the Beaufort scale, winds up to 5 Bft. (10.7 m/s) are in red, winds as of 6 Bft. are colored as shown in the legend below the picture, where all winds of 10 Bft. or higher are in blue. A black arrow indicates that the KNMI QC flag is set, where such winds can be informative to experienced users. Further description can be found at https://scatterometer.knmi.nl/tile_prod/.

eo4society.esa.int/projects/cyms/), by obtaining SAR acquisitions that may be exploited for the resolution enhancement of the operational scatterometer winds (Ni et al., 2022). As wind sources are presented in the same wind speed reference scale after calibration, SAR, scatterometer and ECMWF model winds can be spatially matched with a triple collocation method (Stoffelen, 1998) and the random errors of each of these sources assessed. Moreover, the spatial structure resolved by SAR may be captured in so-called structure functions that may be exploited in scatterometer spatial resolution enhancement.

2.4.1. New and emerging scatterometers

The Chinese Meteorological Administration (CMA) recently launched WindRad (2021), a novel dual-frequency (C- and Ku-bands) rotating fan-beam scatterometer (Li et al., 2019), which has been prepared by exploiting collocated ASCAT and OSCAT2 data in several scientific publications. The novelty implies a somewhat longer commissioning phase than for the more established scatterometer types, e,g., developing beam pattern calibration, extending geophysical model functions, optimizing retrieval and Quality Control (QC) and instrument monitoring codes. EUMETSAT will launch the MetOp-SG SCA scatterometer (Stoffelen et al., 2017a) with cross polarization (VH) in 2024 which, like the cross-polarization channel of the SAR, are capable of measuring extreme hurricane winds (see also section 5.5).

2.5. Microwave imagers/sounders

Microwave (MW) imagers, such as the Special Sensor Microwave - Imager/Sounder (SSMIS) onboard DMSP, the GPM Microwave Imager (GMI), the Advanced Microwave Scanning Radiometer – 2 (AMSR2) onboard GCOM-W, and other similar sensors have been long providing imagery very useful for analyzing tropical cyclone location and structure. They allow a clear determination of TC center, cloud pattern/structure and eyewall replacement cycle features (Fig. 7). These sensors also provide satellite-derived products such as associated precipitation, wind speed, columnar water vapor, and, for sensors with 6–10 GHz channels, Sea Surface Temperature (SST), all of which are also accessed regularly during TC occurrences (see appendix C for links to data).

Recently, the number of satellites carrying these sensors has been decreasing, leading to larger gaps in coverage and time between overpasses. Emerging new MW sensors include the FY-3 series of polar orbiters by the CMA and National Remote Sensing Center of China (NRSCC), which started in 2008 (Zou, 2021). The FY-3E satellite was successfully launched on

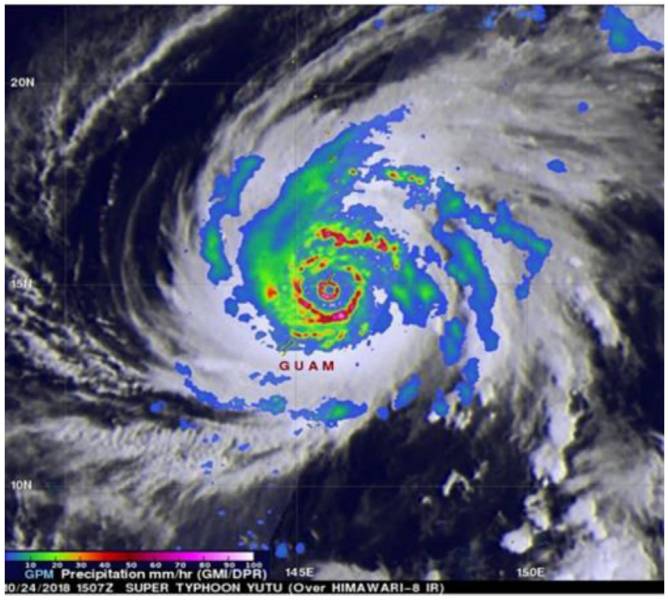

Fig. 7. GPM's GMI/DPR view of Yutu's eye (with storm center location at 146E,15N) and precipitation, on 10/24/2018 at 15:07 UTC. From https://gpm.nasa.gov/gpm-views-powerful-typhoon-yutu.

5 July 2021: it is the fifth of the second generation polar-orbiting meteorological satellites and the first civil early-morning orbital meteorological satellite. The combined FY-3E, FY-3C and FY-3D satellites provide global coverage every 6 h for numerical weather prediction (NWP). The addition of an early morning orbit with FY-3E fills an important observational gap and is expected to improve the accuracy and timeliness of global NWP (Zhang et al., 2022). The FY-3E satellite includes a microwave temperature sounder, a microwave humidity sounder, a dual frequency scatterometer, and an hyperspectral infrared atmospheric sounder. These instruments allow monitoring the three-dimensional structure of the atmosphere, the ocean surface wind vector field, and low-light imaging. The microwave temperature and humidity profiles obtained by the fusion and inversion of the microwave temperature and humidity sounder can penetrate cloud-rain and provide the three-dimensional structure of tropical cyclones.

2.6. Geostationary sensors

The new generation of geostationary satellites includes the JMA Himawari-8 and 9 (since 2014) (Bessho et al., 2016), the NOAA GOES-16, -17, and recently launched GOES-18 (March 2022) (Goodman, 2020), EUMETSAT/ESA Meteosat-9,-10, and −11 (Schmetz et al., 2002), the CMA/NRSCC FY-4 series (Chen et al., 2018), the KMA/KARI COMS (ended in 2021) and the follow-on GK-2A (Kim et al., 2021). The new GEO sensors provide higher spatial and temporal sampling (from 1-min mode to 10 min), very important for monitoring the rapid changes of convective features, storm development and exact location (see section 3 for examples of operational use of the rapid scan modes).

The FY-4B satellite was successfully launched in June 2021. It is the first operational satellite of the new generation of geostationary meteorological satellites. FY-4B and FY-4A (launched in 2016) constitute a geostationary orbit meteorological satellite network system, which allows high-frequency monitoring of atmosphere and clouds, obtains the vertical information of the clear sky and thin cloud regions and generates various physical parameters and quantitative products. KMA launched GK-2A in December 2018, a follow-on satellite to COMS. GK-2A has 16 channels and is a next-generation advanced meteorological imager. GK-2A generates a full disc image every 10 min, and when necessary, it also provides special observation images for a targeted area at 2-min intervals, allowing continuous monitoring of the TC track. Furthermore, GK-2A provides 52 types of basic level-2 meteorological products including sea surface temperature and high-level products for TC analysis.

2.7. Aeolus, wind profiler lidar

Europe has successfully and uniquely demonstrated a new atmospheric wind profiling mission, Aeolus, based on the Doppler Wind Lidar (Stoffelen et al., 2020). Aeolus has a single line of sight (LOS) with a UV laser, hence the orbiting satellite produces a curtain of horizontal LOS wind vector components in a dawn-dusk (6:00/18:00 LST) orbit (Fig. 8). The Aeolus space mission operated for 4 years and recently ended in July 2023. The winds were processed and publicly released in NRT (see Appendix C), and were operationally assimilated by 7 global NWP centers (some listed in Appendix D). For NWP, the winds are aggregated over 90 km in the horizontal and cover the troposphere at about 1 km vertical resolution and the top bins up to 24 km height at 2 km. Molecular winds, covering 75 % of the atmosphere have negligible bias and random error of 4.5 m/s or more, depending on mission phase. The cloud and aerosol winds have lower random error of about 2.5 m/s and cover 10 % of the atmosphere. As Aeolus cannot look through thick clouds, its contributions on cyclones are on the measurement of the otherwise unobserved clear air dynamics around the cyclones. The ESA Aeolus mission, though noisier than specified, achieved its mission goals in terms of NWP impact. The UV laser molecular wind profiles bring very substantial benefit to the several global NWP centers that assessed Aeolus in Observing System Experiments (OSE). ECMWF and other NPW models are furthermore testing Aeolus impact in extreme weather forecasts, such as from tropical cyclones (Garrett et al., 2022; Marinescu et al., 2022; Rennie et al., 2021). More details about the Aeolus mission can be found on a special collection from the Quarterly Journal of the Royal Meteorological Society

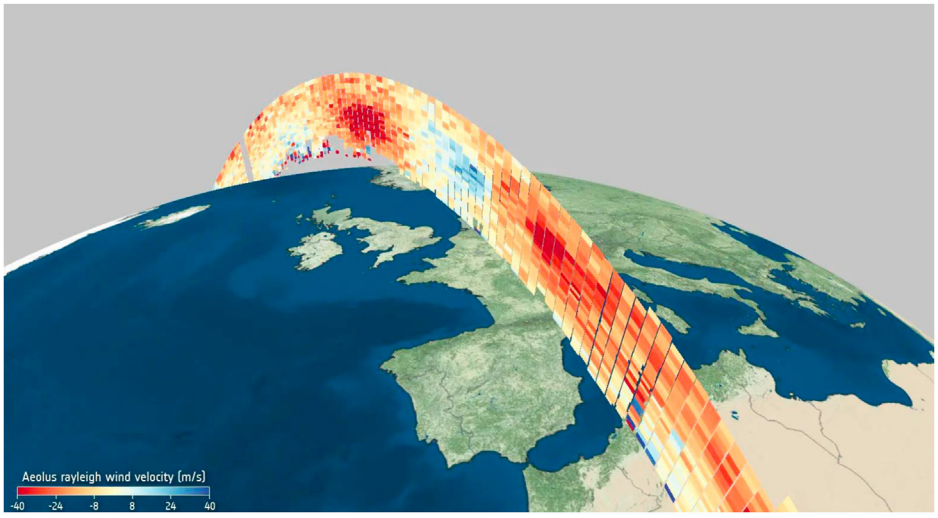

Fig. 8. Horizontal line of sight of the vertical profile for the Rayleigh wind velocity mode from Aeolus 6 May 2020. From https://www.eoportal.org/satellite-missions/aeolus.

(https://rmets.onlinelibrary.wiley.com/doi/toc/10.1002/(ISSN)1477-870X.aeolus). EUMETSAT and ESA are planning an operational follow-on mission, Aeolus-2.

2.8. GNSS reflectometry: CYGNSS

The NASA CYGNSS mission represents a new approach for surface wind measurements in TCs: launched in December 2016, CYGNSS is a constellation of small satellites with inclined low Earth orbits to provide coverage in the tropics with a frequent revisit time (Ruf et al., 2018; 2019). It uses L-band reflectometry to measure ocean surface winds via the existing network of Global Navigation Satellite System (GNSS). There are two main sources of data products (Carreno-Luengo et al., 2021): The University of Michigan (Ruf et al., 2019) and NOAA/NESDIS/STAR (Said et al., 2019; 2021), both distributed by NASA JPL PO.DAAC. CYGNSS surface wind observations suffer from calibration biases due to the transmitted power. These were empirically corrected to obtain wind observations consistent among adjacent tracks and versus other validation sources; some are corrected with latency of ~1 month. The NOAA product includes a track-wise bias correction implemented with short latency (Fig. 9) (Ricciardulli et al., 2021) provides an assessment of different CYGNSS wind products in TCs. The most recent version of the CYGNSS wind dataset (V3.1) includes a recent recalibration of the transmitted GPS power resulting in improved wind retrievals. Also, a new storm-centric wind product has been developed for storm-analyses (Mayers et al., 2023). At this time, CYGNSS wind retrievals are not produced in NRT, limiting the potential use in operations. Within the context of TC observations, CYGNSS is to be considered a proof-of-concept mission.

2.9. Small and cube satellites

Due to the high costs of GEO/LEO satellite sensors, in the last five years or so, a convergence of technological advances in electronic miniaturization, antenna and receiver design, solar arrays, and onboard computing have paved a new path to host microwave sensors on much smaller satellite buses (here referred to as SmallSats). A subset of SmallSats are CubeSats, based on a standardized Cube (1U = 10 cm × 10 cm x 10 cm) that has gained traction as a global form factor for a myriad of applications. This international CubeSat standard has been embraced by hundreds of large and small companies, universities, and government entities and has exploded in terms of innovation and advances. Three current SmallSats missions for TC observations are:

2.9.1. TROPICS

An example of CubeSats potentially solving part of the TC microwave gap is the Time Resolved Observations of Precipitation structure and storm Intensity with a Constellation of SmallSats (TROPICS) mission led by MIT-LL (Blackwell et al., 2018). Seven microwave sounders, with frequency channels between 94 and 205 GHz, were built using a 3U CubeSat satellite with 1U hosting the rotating radiometer payload and the other 2U hosting the electronics, onboard processing and storage, communications, etc. A Pathfinder has been launched in 2021 and has been working well (Blackwell et al., 2022). This is the first time a channel above 190 GHz has flown on a spaceborne cross-track microwave sounder, and this channel clearly reveals fine-scale storm structure near the eyewall and rainbands due to very strong scattering from hydrometeors (Fig. 10).

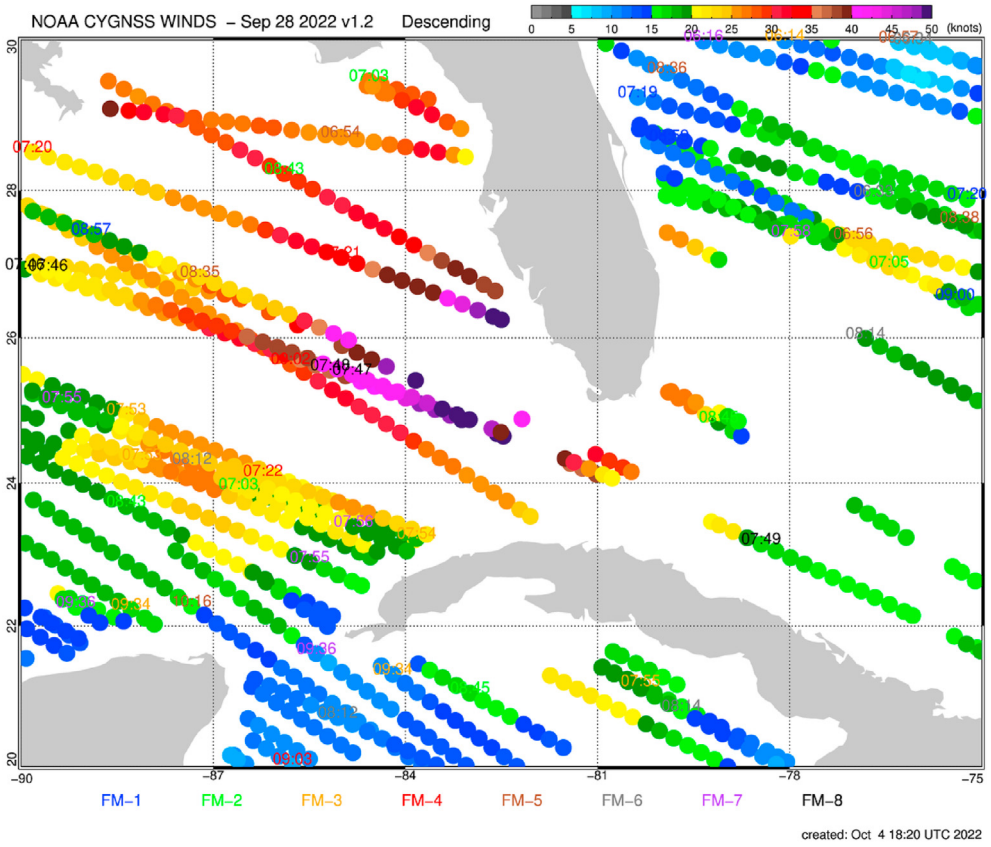

Fig. 9. CYGNSS surface wind speeds for Ian on 28 September 2022 (from https://manati.star.nesdis.noaa.gov). The filled circles represent measurements over the tracks of 8 different receivers (FM-1 to 8), with the UTC time of observation for each track color-coded differently for each receiver.

Four additional TROPICS satellites were inserted into two separate orbital planes (two satellites in each plane, approximately 550 km altitude and 30° inclination) by two dedicated Rocket Lab Electron launches in May 2023. All four TROPICS constellation satellites are now successfully collecting radiometric data and are undergoing a calibration/validation phase. Some "first light" images from TROPICS were released in July 2023 for the first named Atlantic hurricane, Adrian (https://www.nasa.gov/feature/nasas-tropics-offers-multiple-views-of-intensifying-hurricanes). The TROPICS small satellites will undergo a NRT phase funded by NOAA/ONR that will demonstrate the viability of using existing global satellite receiving stations to greatly augment existing operational microwave imagery/soundings temporally for global TC monitoring.

2.9.2. COWVR

The NASA Compact Ocean Wind Vector Radiometer (COWVR) is a microwave radiometer, launched in December 2021, and mounted on the International Space Station (ISS) (Brown et al., 2019; 2021). It is similar to WindSat but with a new and cheaper concept, as only the antenna rotates. It has only channels between 18 and 37 GHz, unlike WindSat that had also 6–10 GHz for SST and better removal of rain in wind algorithm. COWVR data are not publicly distributed yet, but early results for wind speed (rain-free) and direction seem promising. COWVR also observes the rain field in a TC, which can be used to infer TC structure. The use of COVWR for measuring TC winds is limited, as the lack of lower frequency channels (C-band and X-band) makes it difficult to obtain reliable wind speed estimates in precipitation. The first data release by NASA/JPL is planned for mid-2023. Though not yet fully operational, initial limited datasets and imagery files have been made available to JTWC as an early adopter later in 2023, for analysis and validation via both AWIPS and ATCF. Fig. 11 presents an example of the first routine COWVR/TEMPEST imagery made available to the JTWC, for TC Roke off the coast of Okinawa in September 2022.

2.9.3. TEMPEST

Additional CubeSats with microwave sensors such as Temporal Experiment for Storm and Tropical Systems – Demonstration (TEMPEST-D) (Reising et al., 2018), and RainCube (radar) (Radhakrishnan et al., 2022), have clearly demonstrated the fundamental utility of these sensors for TC monitoring. Due to their R&D low-cost limitations, they did not send data down in NRT. This has been updated with the current TEMPEST-1 and SmallSat COWVR, both on the ISS: their data are sent down in NRT via NASA TDRSS communication links and their products have a latency of 1–2 h.

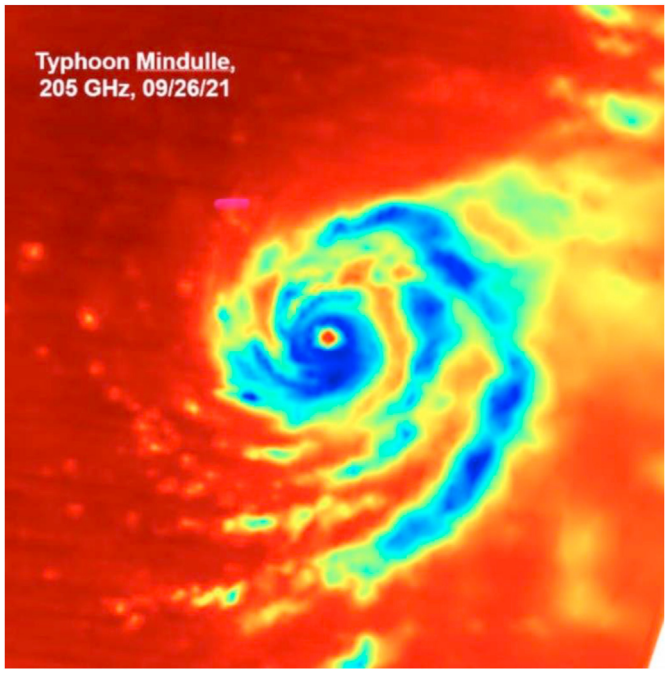

Fig. 10. Time-Resolved Observations of Precipitation structure and storm Intensity from the TROPICS Pathfinder 205-GHz channel imagery at 05:45 UTC on 26 September 2021, when super typhoon Mindulle (WP20) was near peak intensity, with center located at about (137E, 19N).

3. Operational use of satellite sensors for TCs

3.1. Joint Typhoon Warning Center (JTWC)

The JTWC has been utilizing SAR data provided by NOAA STAR via NRL, as part of the TC intensity estimation process, since 2019. Over the course of the past couple of years, new developments including new processing algorithms, automated fix generation and availability of radar cross-section (NRCS) and look angle data within the Automated Tropical Cyclone Forecast (ATCF) system, have increased the confidence in using this data for strong TCs with intensities above 100 knots. In addition to the normalized radar cross sections (NRCS) data available in ATCF, NRL has developed a colorized windspeed plot, which also applies to all other windspeed data, and also contains a values' overlay, enabling rapid estimation of maximum winds and radius of maximum wind (RMW) and wind radii. The main drawback to SAR is the limited availability of the data, with the schedule needing to be coordinated across multiple agencies and foreign partners. However, the process is smooth and JTWC has made use of these data numerous times in the past two to three years, including for recent high-impact TC's such as Hinnamnor (Fig. 12), which provided high confidence intensity (Vmax) data as well as unique insights to TC structure.

JTWC has routine access via the ATCF for both SMAP and SMOS data, and has been using these data routinely since 2019 in tropical cyclone intensity analyses. These have been validated to be highly accurate for tropical cyclone winds above 65 knots, though the 40 km resolution and lack of direction data is a drawback for many systems. JTWC has used data from these sensors on hundreds of occasions to analyze TC intensity, including in some high-profile cases such as TC Mawar on May 23, 2023 May (Fig. 13a). This SMAP pass was relevant to the JTWC in real-time, as it provided confirmation of a RCM-2 SAR pass 45 min later and was slightly higher than the available Dvorak fix estimates, thus providing the JTWC with increased confidence in assigning a 135 kt intensity while it was only 125 nm from Guam and inbound quickly. JTWC has also access, via NRL, to both the NOAA all-weather and REMSS TC-wind measurements for the AMSR2 sensor. Data is available in NRT in ATCF, as noted in the example in Fig. 13b from super-typhoon Hinnamnor on August 31, 2022, which provided high confidence to the 125 kt intensity at this valid time.

Recently, JTWC introduced ProxyVis, a new technique, utilizing multiple shortwave infrared and nighttime visible channels or proxies, to create a nighttime satellite image that approximated daytime visible imagery (Chirokova et al., 2023) (see appendix C). JTWC now has access to Himawari-8 and GOES-W ProxyVis imagery, both in AWIPS and within the ATCF tool. Access to this new enhancement increases confidence to the initial positioning for weak, asymmetric TCs in the development phase; Fig. 14 (Super-typhoon Hinnamnor)

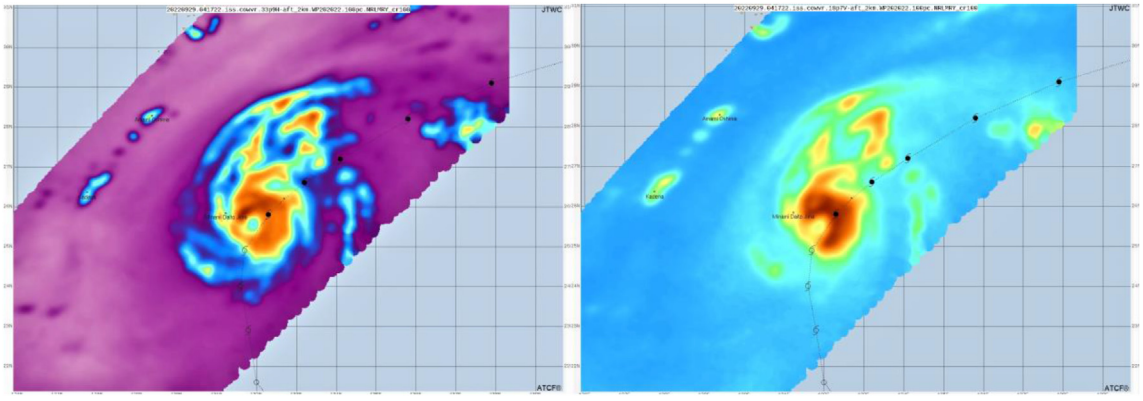

Fig. 11. Example of COWVR images at 33 GHz (left) and 18 GHZ (right) from TC Roke (WP20) on September 29, 2022 at 04:17 UTC, with center located at about (132E, 25.5N) off the coast of Okinawa. This was the first storm that had routine COWVR/TEMPEST coverage available to the JTWC.

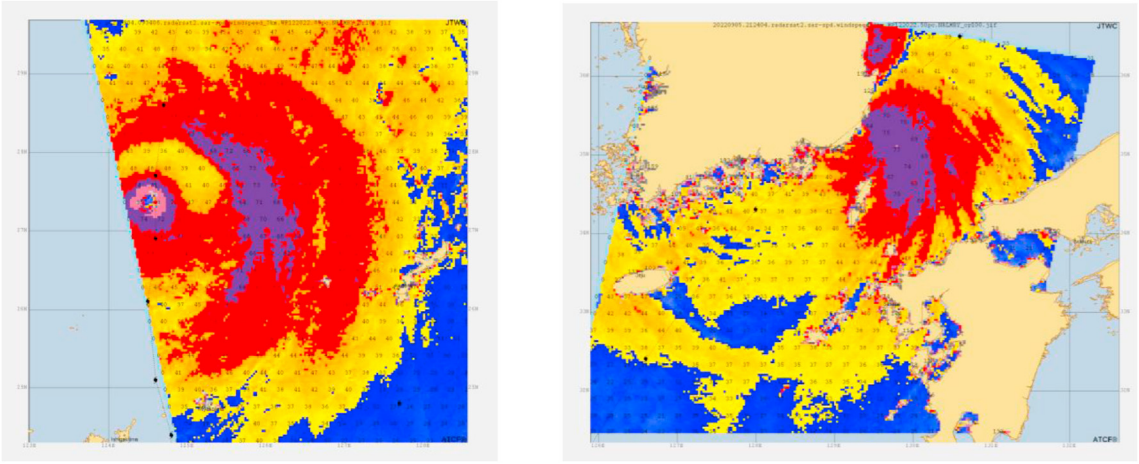

Fig. 12. JTWC/NRL TC wind structure from RadarSat2 SAR for Super-typhoon Hinnamnor (WP12) on September 4, 2022, at 9:34 UTC (left; longitude/latitude range is 123–128.5E, 24.5–29.5N) and September 5 at 21:24 UTC (right; 126-132.5E, 31.5–36.5N). Color coded regions are: yellow = 34 kt, red = 50 kt, purple = 64 kt, pink = 80 kt. Wind speeds (kt) for individual pixels are indicated by the black numbers.

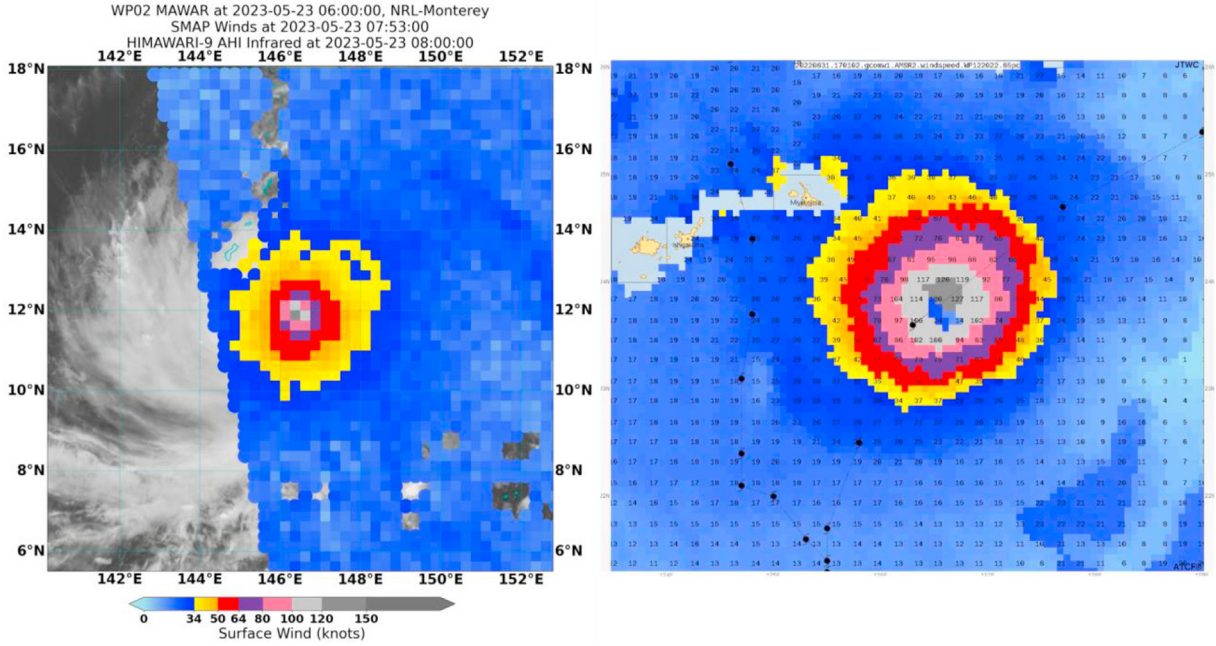

Fig. 13. (left) JTWC/NRL analysis of TC WP02 (Mawar) on May 23, 2023, using SMAP observations at 07:53 UTC, overlapped to Himawari-9 IR image at 8 UTC; (right; longitude/latitude range is 123.5–129E, 21.5–26N) similar JTWC/NRL analysis of NOAA AMSR2 winds for Super-Typhoon Hinnamnor (WP12) on August 31, 2022, at 17:01 UTC.

illustrates an example for a Tropical Storm with the low-level center on the northern side of an area of deep convection, and the low-level banding features highly evident in the ProxyVis imagery, providing increased confidence in the position.

3.2. National Hurricane Center (NHC)

There have been several advances at the NHC in the use of satellite for operational analysis, forecasting, and decision-making in recent years. One is the use of the new generation of GOES satellites (GOES-16 and -18), which cover much of NHC's area of responsibility. Multi-channel RGB products from GOES and Meteosat satellites provide additional capabilities for diagnosing the tropical cyclone environment, including assessing the likelihood of tropical cyclogenesis, intensification and structural changes such as extratropical transition. These products help forecasters assess atmospheric moisture and interactions with mid-latitude troughs, among other features. The GOES satellites offer increased spatial and temporal resolution and numerous additional channels of imagery compared to legacy satellites. For example, full disk imagery is available every 10 min with mesoscale imagery sectors providing 1-min imagery over features of interest, including tropical cyclones. This high-temporal imagery, especially from visible channels, has improved the analysis of

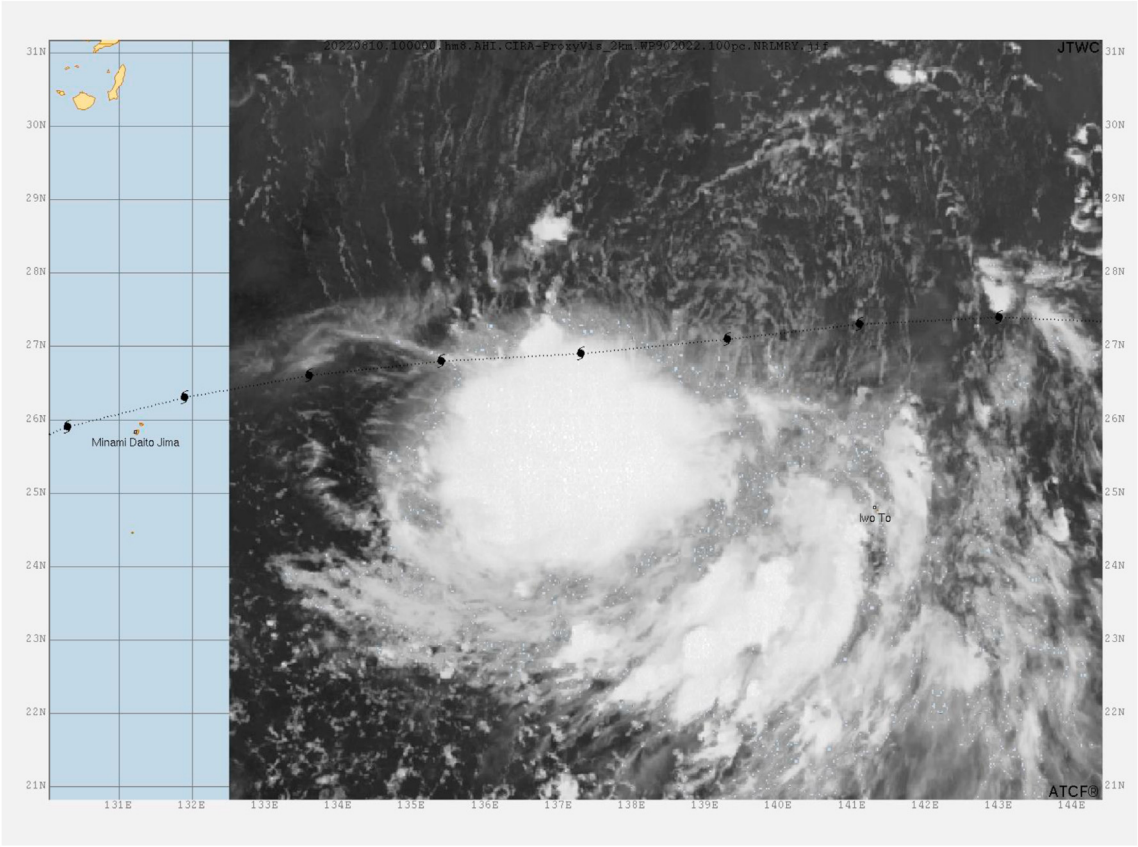

Fig. 14. JTWC ProxyVis imagery of TC Meari (WP09) on August 10, 2022, at 10 UTC, based on Himawari 8.

tropical cyclone center formation and location, which helps forecasters determine when a tropical cyclone has formed to initiate advisories and improve location and intensity analysis via the Dvorak technique (Dvorak, 1975; Velden et al., 2006). The advent of so-called ProxyVis imagery (section 3.1), which provides visible proxy imagery at night by leveraging several channels, has also proved very beneficial for tropical cyclone location and intensity analysis. At NHC, SAR data are at this time being analyzed before incorporating them into real-time and post-storm analysis of tropical cyclones.

3.3. Bureau of meteorology, Australia (BoM)

The BoM complement their use of ASCAT and HSCAT-B and -C scatterometer winds with an increased use of surface winds via SMAP, SMOS, and AMSR2 radiometers and SAR, when available, producing an improved surface wind analysis. This particularly applies to intensity and wind structure (especially gale radii) estimation. The experience of using the collection of sensors in different contexts – formation, intensification, weakening, and extra-tropical transition– has been a part of training programs to ensure consistency across all forecasters. For example, there is increased confidence in using microwave, scatterometry and radiometer imagery to deviate from standard intensity estimates from subjective Dvorak and objective Advanced Dvorak (ADT)/SATCON techniques (Velden and Herndon, 2020). This is particularly the case when traditional techniques are at their weakest such as during formation, covered center patterns, eye-wall replacement cycles and sub-tropical or extra-tropical situations (see example in Fig. 15). The use of Himawari in rapid-scan mode has provided occasional useful insights into convective changes and also cloud rotation for positioning.

3.4. La Reunion, Meteo-France

SAR data are increasingly used in both operations and post analysis although episodic conflicting data in co-located passes (SAR-SAR or SAR-SMAP) need further investigation before forecasters have full confidence in the results. Operational use is facilitated thanks to appropriate SAR diagnostics (wind profiles by quadrants) developed by the STAR team of NOAA (SAROPS website, see Fig. 1) and the CLS/Ifremer teams (see appendix C). Between 2017 and 2020, wind data of 30 SAR overpasses have been compared to independent Regional Specialized Meteorological Center (RSMC) La Reunion best-track estimation. The results show overall good agreement (Fig. 16). SAR winds data are also helpful to assess the inner core wind structure (storm and hurricane winds radii along with the radius of maximum winds).

3.5. Canadian Hurricane Center (CHC)

Forecasters at the CHC are primarily faced with the challenges associated with forecasting extratropical transition (ET)

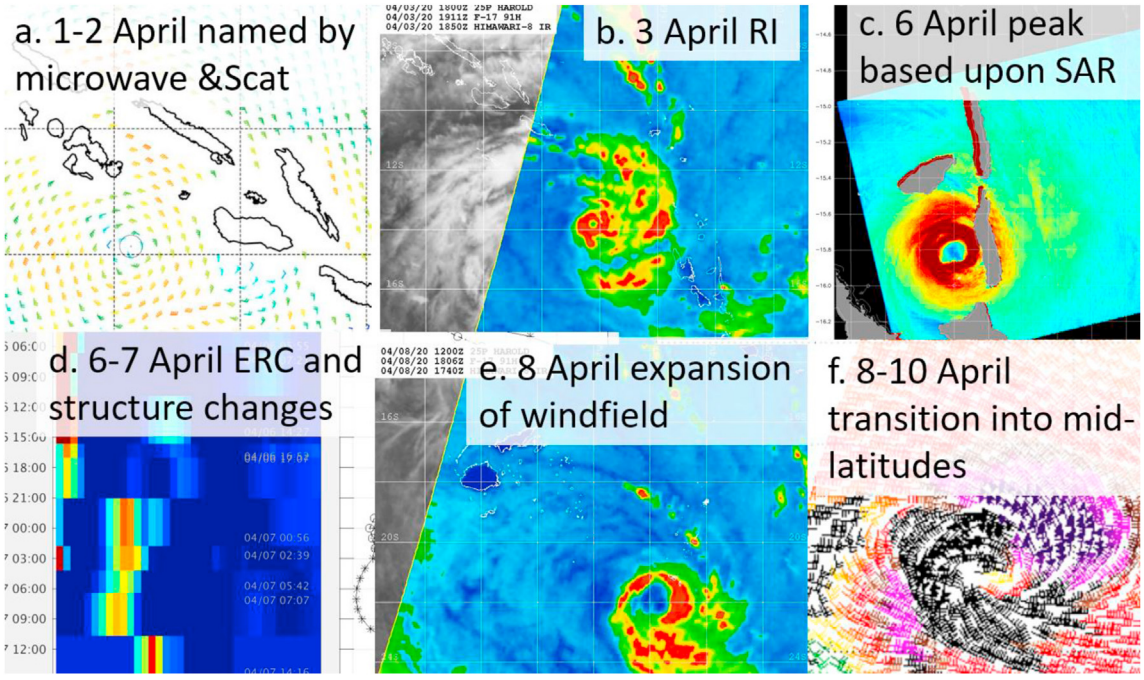

Fig. 15. Example of use of different satellite sensors within the lifetime of TC Harold, 1–10 April 2020: (a) Genesis named based on MW radiometers and scatterometers (displayed here); (b) Rapid Intensification based on Himawari-8 and SSMIS; (c) Fine TC structure during peak from SAR; (d) Microwave-based Probability of Eyewall Replacement Cycle (M-PERC model, CIMSS; the ring score is displayed as a function of radial distance (horizontal) and time (vertical); see https://tropic.ssec.wisc.edu/real-time/archerOnline/web/index_erc.shtml for more information on M-PERC); (e) TC Expansion phase from Himawari-8 and SSMIS; (f) Extra-Tropical transition as seen from ASCAT.

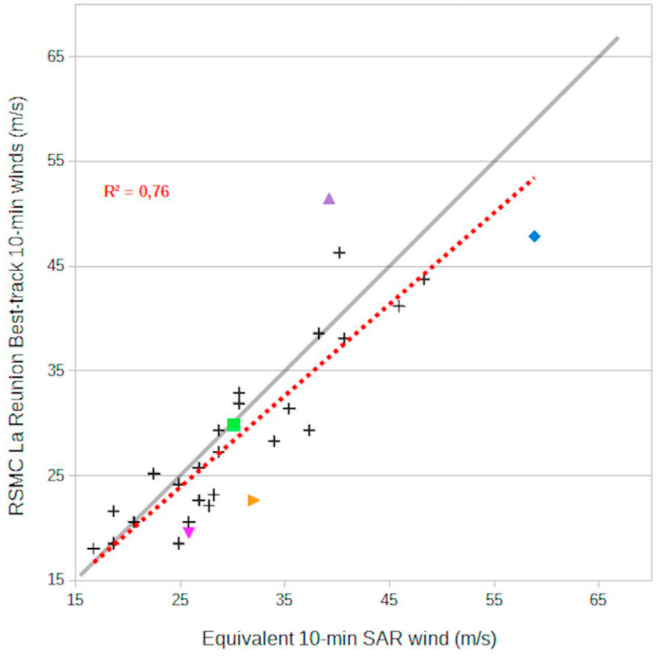

Fig. 16. Comparison between equivalent 10-min SAR maximum winds and RSMC La Reunion Best-track estimates for 30 SAR overpass in 2017–2020.The red line is the linear fit with correlation R^2, and the color symbols refer to some sample TC cases: Carlos (magenta), Galena (green), Francisco (orange), Joaninha (purple), and Idai (blue), (figure adapted from Duong et al., 2021).

of the tropical cyclones in the western North Atlantic Basin. As with all operational forecast agencies, satellite imagery and data are crucial to diagnose the intensity and structure changes of the approaching storms. In recent years the Radarsat Constallation Mission (RCM) trio of polar-orbiting SARs have offered more frequent 'captures' of ET events in the CHC forecast area of responsibility (https://www.asc-csa.gc.ca/eng/satellites/radarsat/). North Atlantic coverage has been augmented by Sentinel NASA imagery as well (https://www.earthdata.nasa.gov/sensors/sentinel-1-c-band-sar). A recent example of the utility of these data was during the grazing passage of Post-Tropical Storm Alex in early June of 2022. The real-time information helped reveal a trajectory of the storm further north than the one predicted by most numerical models, and meteorologists were able to make some short-term forecast adjustments. The CHC is collaborating with other TC warning centers to study and share knowledge of detailed storm structure information made possible by these SAR instruments in recent years. A substantial collection of imagery and data has become available since 2016 via the SAROPS Tropical Cyclone Winds program website and deserves further analysis. Many events include samplings during the ET phase. Research about ET cyclones, and their transition phases in all different basins, will benefit from the information provided by these data. The Sentinel instrument output shown in Fig. 17 highlights an example of some of the detailed features during the ET of Hurricane Teddy in 2020.

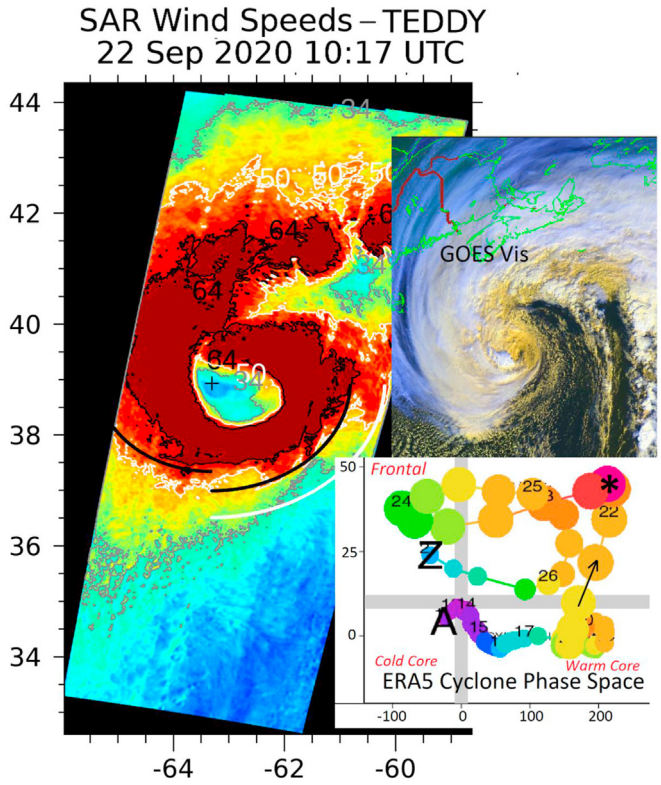

Fig. 17. Example of use of Sentinel SAR 10m winds during the Extra-Tropical transition of Hurricane Teddy (2020) south of Nova Scotia, Canada. The asterisk in the Cyclone Phase Space (Hart, 2003) inset (lower right) denotes the corresponding phase of the storm in the ECMWF Reanalysis (ERA).

3.6. Japan Metereological Agency (JMA)

JMA began to use several satellite products in operational TC analysis after IWTC-9. At the Agency, atmospheric motion vectors (AMVs) are derived from Himawari-8 full-disk imagery captured every 10 min and imagery from target observations conducted every 2.5 min (Otsuka et al., 2018). Since July 2017, JMA has used AMV-based Sea Surface Winds (ASWinds) data computed using low-level AMVs to evaluate surface winds around TCs (Nonaka et al., 2019). Since the 2019 TC season, the qualities of ASWinds in the vicinity of TCs have been shared with users based on statistical verification with reference to ASCAT sea surface wind data, with verification results provided in the RSMC Tokyo-Typhoon Center Annual Report. Another use of Himawari-8 AMV data involves JMA's internal application of high-level AMVs in monitoring of upper-tropospheric winds in the vicinity of TCs, which reveals the characteristics of TC secondary circulation or interaction between TC winds and environmental winds. JMA has also introduced RGB compositing using imagery from Himawari-8 IR (wavelength: 10.4 μm) and three WV bands (6.2, 6.9 and 7.3 μm) to observe wet/dry areas in the mid/upper troposphere. In addition, Himawari-8 Near-IR (1.6 μm) imagery, which is suitable for identifying lower clouds, has been adopted to improve accuracy in determining low-level TC rotation centers.

3.7. Philippine Atmospheric, Geophysical and Astronomical Services Administration (PAGASAA)

Himawari-8 received via satellite broadcast (HimawariCast) is currently the only geostationary satellite data being used operationally at PAGASA. During tropical cyclone events, it is used primarily for Dvorak Analysis and Early Dvorak Analysis (EDA). Early Dvorak Analysis is a pre-storm intensity analysis technique introduced by the RSMC – Tokyo.

3.8. India Meteorological Department (IMD)

The INSAT 3DR RAPID scan mode (https://mausam.imd.gov.in/responsive/satellite_rapidscan.php) is 4.5 min, and the number of scan lines over a given coverage region and the number of repetitions of the selected region can be programmed for scanning. This allows high temporal resolution and helps in better evaluation of cloud characteristics including convection boundaries, determination of center, enhanced diagnosis of eye and eye-wall characteristics including diameter, shape, evolution of eye as well as the spiral band characteristics. All these provide a better estimate of intensity, location of center and structural parameters of a tropical cyclone, and estimating the region of higher precipitation and stronger winds.

3.9. China Meteorological Administration (CMA)

FY satellites provide cloud images with high temporal and spatial resolution in real time. In order to better use the satellite cloud images to monitor tropical cyclones, the National Meteorological Center (NMC) has explored the application of machine learning in tropical cyclone vortex detection. Recent analyses proved that this technology has excellent TC vortex detection ability: the correct recognition rate of tropical cyclone with intensity below severe tropical storm (STS) level is 40–80 %, above STS level is more than 90 %, and above typhoon level is very close to 100 %. Additional recent advances were achieved by the FY-4B fast scanning, 1 min 250-m resolution, applied to monitor the development of small-scale convection in the core area of the tropical cyclones and the mutual interaction of multiple tropical cyclones. The water vapor transportation and distribution, development and movement of convective clouds over TCs during the precipitation process are also monitored in real-time by FY-4B satellite cloud image animation.

3.10. Korea Meteorological Administration (KMA)

The GK-2A satellite products at KMA describe the fine details of typhoon structures which contribute to TC analyst's decision-making. The National Meteorological Satellite Center basic TC information includes the TC center, intensity, wind radii and moving information based on the Dvorak techniques. New imagery bands, including the SWIR (3.8 mm) for the night-time low-level cloud circulation and several RGB composites with better spatial-temporal resolution, are giving more confidence in estimating the storm center and intensity. KMA produces their own web-based satellite imagery analysis

system with KMA-ADT: this objective ADT uses GK-2A observations to derive storm features. The National Meteorological Satellite Center (NMSC) at KMA also provides rapid scan service using "Local Area observation mode" which covers a 1000 km x 1000 km moveable area every 2 min.

4. Updates on assimilation of satellite sensors data

TC forecasting is very sensitive to the initial conditions. The data assimilation system is designed to maximize the exploitation of many different types of satellite observations (e.g., winds, temperature, humidity, clouds, and surface parameters), which provide highly accurate, up to date and continuously improving initial conditions. Throughout the life cycle of a tropical cyclone, satellite observations play key roles: a) During the genesis of a storm (e.g. off the west coast of Africa in the case of Atlantic cyclones), signals in the surface pressure or wind field can be very subtle, but satellites successfully identify the environmental conditions of SST, convection, mid-level humidity and low wind-shear that inform the likelihood of storm development in the forecast model; b) Once a storm is mature in the open ocean, the assimilation exploits a huge variety of different satellite technologies, operating at different frequencies, to constantly monitor intensity and structure, and communicate any changes to the forecast model; c) In many cases accurate predictions of trajectory and landfall depend on a highly accurate knowledge of the large-scale environment and steering flow (possibly the most famous example being Hurricane Sandy in 2012). For this a constellation of infrared sensors on board LEO and GEO satellites are used to infer (by tracing clouds and humidity) a highly detailed description of the AMV wind field.

Recent progress in data assimilation by some operational forecast centers is described below.

4.1. Met Office UK

In terms of new instruments, during 2018–2022, the microwave imager (MWRI) onboard the Chinese FY-3 series have been assessed and incorporated into operations in the UK Met Office, along with the U.S. GOES-ABI infrared imager. The use of active sensors has also been extended in this period. Optimal use of observations requires good estimates of their uncertainty. Improvements to uncertainty estimates for AMVs and GNSS Radio Occultation (GNSSRO) observations have been implemented. A new source of wind profiles comes from Aeolus, the first Doppler Wind Lidar (DWL) instrument in space. Following assessment of the new instrument and demonstration of positive forecast impact, the Met Office began assimilating DWL data in 2020. Other new instruments include additional GNSSRO receivers from the FY-3 series of satellites and the commercial SPIRE satellite constellation. The use of these additional receivers significantly increases the number of assimilated GNSSRO profiles.

4.2. European Centre for Medium-Range Weather Forecasts (ECMWF)

Operating globally at a spatial scale of around 9 km, the ECMWF system is not specifically designed with the forecasting of tropical cyclones in mind. Yet the ECMWF forecasts of these severe life-threatening phenomena are widely regarded to be one of the best sources of information available to decision makers charged with the implementation of civil protection strategies around the world.

One ongoing challenge during the genesis phase of a storm is to discriminate the small amplitude signals in satellite pixels potentially confused by the presence of cloud and aerosol intrusion: these are now being addressed with the development of highly sophisticated cloud and aerosol detection schemes. Within the core of the storm in the mature phase, the assimilation relies primarily on microwave radiance observations to update humidity, cloud and precipitation conditions. Air-sea interactions below the storm are monitored with low-frequency, and hence weather-penetrating, scatterometers and radar altimeters. A present major focus is coupling the atmospheric data assimilation system to the ocean data assimilation. In this way scatterometers' information of surface stress can be

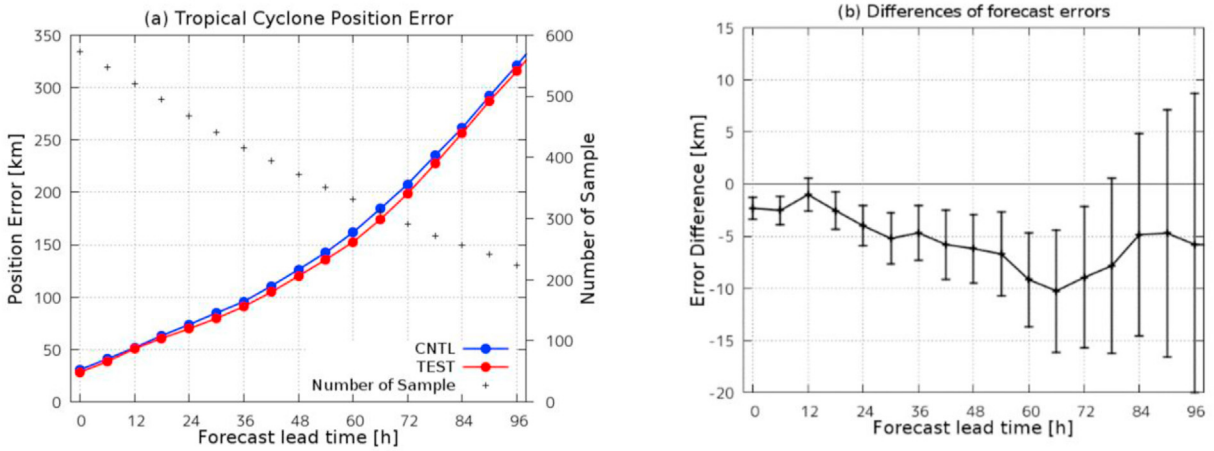

Fig. 18. (a) Average TC track forecast errors for the JMA all-sky assimilation experiments. The red and blue lines are for TEST and CNTL, respectively, and dots represent sample data numbers. (b) Forecast error differences between TEST and CNTL. Error bars represent a 95 % confidence interval.

used to infer changes to the SST forced by vertical mixing (e.g. the cold wake of a cyclone), as temperature of the surface layer of the ocean is known to be a key factor in rapid intensification (or not) of a storm. Additional wind information is provided by the Atmospheric Motion Vectors (AMV) from GEO or LEO satellite observations and more recently by wind profiles from the Aeolus Doppler wind lidar. The immediate development frontier for ECMWF is to move the operational forecasting and data assimilation system down to even finer spatial resolution. The next upgrade will likely see the headline model resolution move to around 4–5 km, and there are already experiments with prototype systems operating globally at 1.25 km. Looking ahead, the planned advanced satellite systems will support this evolution to forecasting at smaller spatial scales and bringing expectations of more accurate tropical cyclone predictions.

4.3. La Reunion Meteo-France

An example of the impact of SAR winds assimilation for TC forecast was assessed by using a 3D-Var assimilation scheme and the convection-permitting limited area model AROME- OI (non-operational version) for two TC cases (Gelena and Idai from the 2018/2019 Southern Indian Ocean TC season). Results are discussed in (Duong et al., 2021).

4.4. Japan Metereoplogical Agency (JMA)

JMA operational NWP global model relies on an all-sky microwave radiance assimilation scheme for microwave imagers and microwave water vapor sounders (Kazumori and Kadowaki, 2017), which incorporates outer-loop iterations for the model state trajectory updates in the 4D-Var minimization process for effective assimilation of cloud and precipitation, introduced in December 2019. JMA recently applied the all-sky assimilation scheme to the radiances around 183 GHz from Suomi-NPP, NOAA20/ATMS, DMSP-F17, F18/SSMIS and Megha-Tropiques/SAPHIR. In addition, assimilation of radiances from FY-3C/MWHS-2 for all-sky conditions was commenced. These latest developments were implemented into JMA's operational global NWP system in June 2021. Fig. 18 displays results from all-sky assimilation experiments versus control, and shows that average TC track forecast errors decreased over the whole forecast range up to 96 h. The data assimilation experiments indicated improvement of first-guess water vapor fields for the lower troposphere and the forecast field of geopotential height at 500 hPa, sea level pressure, and wind speed at 850 hPa up to a forecast range of 120 h. These outcomes indicate that all-sky assimilation for humidity sounders also has positive impacts on temperature and wind fields due to the tracking effect of 4D-var (Geer et al., 2014).

4.5. China Meteorological Administration (CMA)

CMA NWP model implemented several assimilation updates: both high spatial and temporal resolution observations such as infrared hyper spectral atmospheric sounding, microwave radiometer, ocean surface wind of HY-2 satellite, as well as the intelligent round-trip sounding (He, 2020) and airborne dropsonde target observation data were fed into CMA 4D-VAR parallel system. These additions effectively improved the ability of the initial value field of numerical prediction to describe the three-dimensional mesoscale structure of typhoons and their environments. In recent years, the National Meteorological Center (NMC) has also explored the application of machine learning using these high temporal and spatial resolution satellite images in real time for tropical cyclone vortex detection (Wang et al., 2023).

5. Newly launched and planned sensors

5.1. OSCAT-3 on OceanSat-3

ISRO launched the third of its Ku-band OSCAT scatterometers on OceanSat-3 in November 2022, on a sun-synchronous 12 a.m./pm orbit. Compared to its Ku-band predecessor ScatSat-1, OSCAT-3 has the added capability of high-resolution mode (6.25 km sampling). The data are not yet operational.

5.2. Sounder of MeteoSat Third Generation

In December 2022 EUMETSAT launched the first of its MeteoSat Third Generation (MTG) satellites (Holmlund et al., 2021), but the data are not operational yet. MTG will provide better resolved imaging and sounding capability, with real-time data on the location and intensity of lightning flashes and improved monitoring of key meteorological parameters such as water vapor, temperature and clouds at higher resolution, precision, using new spectral measurements, particularly relevant for African and east Atlantic areas.

5.3. MWI (Weather-System Follow-On radiometer)

The US Department of Defense Weather System Follow-on will have a MW Imager (MWI). MWI is based on WindSat's legacy, and includes 10–89 GHz channels, but will not have the lower frequency (C-band) channel. It is scheduled to be launched in 2024, on a sun-synchronous 6 a.m./pm orbit similar to WindSat. The presence of fully polarized channels will allow ocean wind vector retrievals with accuracy similar to WindSat. These will mostly be only in rain-free areas as MWI lacks the C-band channel, but an all-weather X/K-band wind algorithm will be explored. Additional simultaneous retrieval capabilities may include precipitation rate, columnar water vapor, liquid cloud water, SST, and sea ice coverage.

5.4. AMSR3

Developed by JAXA as a follow-on mission of the AMSR series, AMSR3 is a microwave scanning radiometer similar to AMSR2: it will include 11 frequencies between 6.9 and 183 GHz (new channel). AMSR-3 on GOSAT-GW is

scheduled to be launched within the Japan Fiscal Year 2024 (April 2024–March 2025). It will provide simultaneous retrievals of all-weather ocean surface wind speeds (including in TCs), precipitation rate, columnar water vapor, cloud water content, SST, and sea ice.

5.5. SCA on MetOP-SG-B, cross-polarized scatterometer

SCA is a new planned EUMETSAT C-band scatterometer (Stoffelen et al., 2017a). The design is similar to ASCAT but will include new cross-polarized (VH/HV) channels, to address the ASCAT VV-pol saturation at high winds. Due to the high sensitivity of the cross-pol channels to high winds (similarly to SAR cross-pol), the SCA scatterometers will be able to retrieve wind vectors in the hurricane force regime. The first SCA in a series of three will be launched on the Second Generation of EUMETSAT MetOp-SG-B1: the launch date is still fluid, and it is currently expected by the end of 2025. Two more SCAs (B2 and B3) will be launched in the following years, planned to cover until 2045. Similar to ASCAT, the SCA will be on a sun-synchronous orbit at 9:30 a.m./pm.

5.6. MWI on MetOP-SG-B

The MetOp-SG-B platforms will also include a multi-purpose MW imager, MWI, with 18 frequency channels between 18 and 183 GHz. MWI on MetOp-SG will retrieve ocean surface wind speed, precipitation (liquid and frozen), columnar water vapor, sea ice coverage, as well as temperature and humidity soundings.

5.7. ESA Harmony 10

For the longer-term, in 2029 the European Space Agency (ESA) is planning the Earth Explorer 10 Harmony mission, which consists in two receive-only SARs, using Sentinel 1D as transmitting source. They will deliver km-scale OSVW, wave and ocean current vector information in association with Sentinel-1 SAR images. Harmony 10 also includes a multi-spectral multi-perspective tandem Thermal Infrared Imager to infer cloud top dynamics.

5.8. CIMR

The ESA/EUMETSAT is planning to launch the Copernicus Imaging Microwave Radiometer CIMR in 2028. This radiometer will feature 5 frequency channels in full polarization (equivalent to 30 channels), the lowest in L-band (1.4 GHz), and the highest in Ka-band (37 GHz). A high spatial resolution consistent to 7-m antenna will allow high spatial resolution of 4 km at 37 GHz, but decreasing resolution with frequency (50 km at 1.4 GHz). CIMR will be on a sun-synchronous orbit at 6 a.m./pm, and will provide observations on a very large swath of 1900 km, covering the polar zones without gap. It will provide retrievals of all-weather ocean wind vector (including in TCs), SST, sea surface salinity, as well as ice coverage, and soil moisture.

6. Summary and concluding remarks

In this article we provided the most recent updates on space-based observations of Tropical Cyclones, as reported at the WMO IWTC-10 meeting (WMO, 2022). The past four years saw an increased use of SAR, SMAP/SMOS, and AMSR2 winds: these are minimally affected by rain and are particularly useful for wind radii determination, tracking intensification, and generation of automated TC Fixes in NRT. Major progress was achieved with the capability of the high-resolution SARs which provide an unprecedented view of the storms' core, and identification of the Radius of Maximum Wind.

There are currently several challenging aspects associated with remote sensing of TCs. The loss of several active/passive sensors (e.g. ASCAT-A, ScatSat, and WindSat) is concerning for the operational community. Additional microwave imagers/sounders are sorely needed by both the operational and research communities. Current satellite data for TC monitoring presents some coverage gaps: most LEO satellites are sun-synchronous and cover 6:00/18:00, 9:30/21:30 and 12:00/00:00 Local Solar Time. Ideally, future sensors could be planned to fill these observational gaps.

For operational users, time-constraints limit the utilization of the increased amount of satellite data products available from different providers: developing a centralized and a unified visualization platform with fast navigation is desirable. The long latency of some datasets might also limit the use in TC operations. Occasionally, conflicting information from different sensors or algorithms results in a decreased confidence in these satellite data. As microwave satellite observables (radiances or backscatter) cannot provide absolute wind speed references to a good physical accuracy, further efforts in establishing a common and consistent set of in-situ references is needed for calibration of all extreme-wind satellite products and verify their uncertainty. Unified efforts are encouraged by satellite data providers and researchers to perform/share broad validation efforts using consolidated ground truth data, coordinate aircraft/satellite sensors campaigns, and assign uncertainty range to data from each sensor.

In-situ data from airborne sensors on air reconnaissance flights are available mostly in the Atlantic Ocean (Holbach et al., 2023), while all other basins rely almost exclusively on satellite data. For operational users in these other ocean basins, it is of outmost importance to get prompt access to any new satellite sensor useful for TC analysis in NRT, even if still experimental.

Despite these remaining challenges, the recent years saw a remarkable progress in space-based monitoring of TCs, and promising new missions are planned in the near future. The new generation of the three SCA scatterometers on MetOP-SG-B (2025–2045) is expected to bring a major advancement in TC analysis, as they will include cross-polarized C-band

channels sensitive to high winds. The new generation of GEO sensors provides higher spatial, temporal (from 1-min mode to 10 min), and spectral resolution. GEO/LEO satellites are expensive (several $100M-$1B or more). Small satellites and Cube-Sats such as COWVR and TROPICS provide cheaper alternatives. At this time, they are considered proof-of-concept missions, with limited provisioning of NRT data, but recent progress on data latency should allow operational use. These experimental sensors might also lead the way for a new generation of operational sensors.

Data availability statement

This publication describes multiple datasets, which are openly available, though for some registration is required. A list of the links where these datasets are available is provided in Appendix C.

Acknowledgments

L. Ricciardulli acknowledges the support of NASA Ocean Vector Wind Science Team contract 80HQTR19C0003. We are very grateful to the contributions on operational updates from Michael Brennan (National Hurricane Center, USA), Ryo Oyama (Japan Meteorological Agency), and Chunyi Xiang (China Meteorological Administration).

Appendix A. List of acronyms

ADT/SATCON Advanced Dvorak Technique/SATellite CONsensus
AMSR Advanced Microwave Scanning Radiometer
AMSU Advanced Microwave Sounding Unit
ASCAT Advanced Scatterometer
AMV Atmospheric Motion Vectors
ASWinds AMV-based Sea-surface Wind
ATCF Automated Tropical Cyclone Forecasting
ATMS Advanced Technology Microwave Sounder
AWIPS Advanced Weather Interactive Processing System
BT Best Track
CDR Climate Data Record
CHC Canadian Hurricane Center
CIMR Copernicus Imaging Microwave Radiometer,
CIRA Cooperative Institute of Research in the Atmosphere
CLS Collecte Localisation Satellites
CMA Chinese Meteorological Administration
COMS Communication, Ocean and Meteorological Satellite, South Korea
COWVR Compact Ocean Wind Vector Radiometer
CYGNSS Cyclone Global Navigation Satellite System
DMSP Defense Meteorological Satellite Program
DWL Doppler Wind Lidar
ECMWF European Centre for Medium-Range Weather Forecasts
EDA Early Dvorak Analysis
ESA European Space Agency
ET Extra-Tropical
EUMETSAT European Organization for the Exploitation of Meteorological Satellites
GCOM-W Global Change Observation Mission for Water
GEO Geostationary Earth Orbit
GK-2A GEO KOMPSAT-2
GMI GPM Microwave Imager
GNSS Global Navigation Satellite System
GNSSRO GNSS Radio Occultation
GOES Geostationary Operational Environmental Satellite
GOSAT-GW Global Observation Satellite for Greenhouse gases and Water
GPM Global Precipitation Mission
HSCAT HY- Scatterometer
HWRF Hurricane Weather Research and Forecasting model
IFREMER French Institute for Ocean Science
IMD Indian Meteorological Department
INSAT Indian National Satellite System
IR Infrared
ISRO Indian Space Research Organisation
ISS International Space Station
IWSATC International Workshop on Satellite Analysis of TCs
JAXA Japanese Aerospace Exploration Agency
JMA Japan Meteorological Agency
JPL Jet Propulsion Laboratory
JTWC U.S. Joint Typhoon Warning Center
KARI Korea Aerospace Research Institute
KMA Korea Meteorological Agency
KNMI Royal Dutch Meteorological Institute
LEO Low Earth Orbit
LOS Line of sight
LST Local Solar Time
MetOp EUMETSAT Meteorological Operational Satellite
MetOp-SG MetOp-Second Generation
MIT-LL Massachusetts Institute of Technology – Lincoln Lab
MTG MeteoSat Third Generation
MW Microwave
NASA National Aeronautics and Space Administration (USA)
NCEP U.S. National Centers for Environmental Prediction
NESDIS National Environmental Satellite, Data, and Information Service
NHC U.S. National Hurricane Center
NISAR NASA-ISRO Synthetic Aperture Radar
NOAA National Oceanic and Atmospheric Administration
NPP National Polar-orbiting Partnership
NRCS Normalized Radar Cross Section
NRL U.S. Naval Research Laboratory
NRSCC National Remote Sensing Center of China
NRT Near Real Time
NSOAS National Satellite Ocean Application Service, China
NWP Numerical Weather Prediction
OSCAT OceanSat scatterometer
OSE Observing System Experiment
OSI SAF Ocean and Sea Ice Satellite Application Facility
OSVW Ocean Surface Vector Wind
PAGASA Philippine Atmospheric, Geophysical and Astronomical Services Administration
PMW Passive Microwave
PO.DAAC Physical Oceanography Distributed Active Archive
R34 34 kt (gale force) wind radii
RCM Radarsat Constellation Mission
REMSS Remote Sensing Systems
RI Rapid Intensification
RMW Radius of Maximum Wind
RSMC Regional Specialized Meteorological Center
SAPHIR Sounder for Probing Vertical Profiles of Humidity
SAR Synthetic Aperture Radar
SCA MetOp-SG scatterometer
SFMR Stepped Frequency Microwave Radiometer
SMAP Soil Moisture Active and Passive (NASA mission)
SMOS Soil Moisture and Ocean Salinity (ESA mission)
SSMIS Special Sensor Microwave Imager/Sounder
SST Sea Surface Temperature
TC Tropical Cyclone
TEMPEST Temporal Experiment for Storm and Tropical Systems
TROPICS Time Resolved Observations of Precipitation
VIS Visible

Appendix B. Main features of currently operating satellite sensors for TC observations

Type	Sat/sensor	Agency	Launch	Freq (GHz)	Orbit	Swath Width (km)	All-weather winds	Wind Res. (km)	Comments
SAR	Sentinel 1A	ESA	2014	5.4	6:00 (D)	80–400	Y	0.1–3	1-min sustained winds; Might have small bias in very intense rain.
	RadarSat2	CSA	2007	5.4	6:00 (D)	20–500	Y	0.1–3	
	RCM 1,2,3	CSA	2019	5.4	6:00 (D)	20–500	Y	0.1–3	
	GF-3	CNSA	2016	5.4	6:00 (D)	10–650	Y	n/a	
L-band Winds	SMAP	NASA	2015	1.4	6:00 (D)	1000	Y	40	10-min sustained winds; Mostly unaffected by rain.
	SMOS	ESA	2010	1.4	6:00 (A)	1000	Y	50	
X/C band Radiometers	AMSR2 TC-winds	JAXA	2012	6–11	13:30 (A)	1450	Y	50	Might have small residual bias in intense rain rate; 10-min sustained winds.
	AMSR2 Radiance			6–89			Y	5–50	Highest resolution at high frequency channels.
Scatterometers	ASCAT-B ASCAT-C	ESA	2012 2018	5.3	9:30 (D)	2x550	Y	12–50	Rain impact mostly at low winds (<5 m/s); Calibration of high winds differs for each data provider; 10-min sustained winds
	HY-2B HY-2C	NSOAS	2018 2020	13	6:00 (D)	1300	NO	25–50	Significant rain impact; Positive bias at low winds, negative bias at high winds; 10-min sustained winds.
	CFOSat	CNSA/CNES	2019	13	7:00 (D)	1000	NO	10–50	Rain impact similar to HY-2B,C Rotating Ku-band fan-beam: multiple views allow more accurate wind retrievals; 10-min sustained winds
	WindRad	CMA	2021	5.3 13.3	5:40 (D)	1200	Y	10–25	Dual frequency (C-Ku) scatterometer: Capability at high winds and all-weather; 10-min sustained winds

(*continued*)

Type	Sat/sensor	Agency	Launch	Freq (GHz)	Orbit	Swath Width (km)	All-weather winds	Wind Res. (km)	Comments
MW Imagers/Sounders	SSMIS 16 SSMIS 17 SSMIS 18	US DoD	2003 2006 2009	19–183	6:20 (D) 6:40 (D) 4:50 (D)	1700	NO	15–50	MS Imagers; Temperature sounder failed on F-18; F-16/17 temperature sounder noisy
	GPM GMI GPM DPR	NASA	2014	10–183 13 35	Precess.	930 125 245	NO n/a	5–30 0.25 V 5.0H	MW Imager Precipitation radar
	ATMS 1.NOAA-20 2.SNPP	NOAA/NASA	2017 2011	23–185	13:25 (A) 13:25 (A)	2300	n/a	16–75	MW sounder
	AMSU-A/B 1.MetOp-B 2. MetOp-C 3.NOAA18 4.NOAA19 5. Aqua	NOAA	2012 2018 2005 2009 2002	23–89	9:30 (D) 9:30 (D) 8:05 (D) 7:30 (D) 13:30 (A)	2250	n/a	48	MW sounder N19 ch8 noisy
	MHS 1.MetOp-B 2. MetOp-C 3.NOAA18 4.NOAA19	EUMET SAT	2012 2018 2005 2009	89–190	9:30 (D) 9:30 (D) 8:05 (D) 7:30 (D)	2180	n/a		MW sounder N18 MHS failed 2018
	MWHS/ MWTS 1.FY-3C 2.FY-3D 3.FY-3E	CMA	2013 2017 2021	50–190	8:20 (A) 13:29 (A) 5:40 (A)	2700	n/a		MW humidity sounder and MW T sounder
	MWRI 1.FY-3C 2.FY-3D 3.FY-3E	CMA	2013 2017 2021	10–190	8:20 (A) 13:30 (A) 5:40 (A)	1400	NO		MW Imager
Small Sats	TROPICS	NASA	2021–2023	90–205	2:00 (A)	2000	n/a		Engineering qualification model for the NASA TROPICS mission (Pathfinder, 2021), and four additional satellites launched in 2023
	ISS-COWVR	NASA	2021	18–34	Precess.	1000	NO	12–30	Low-cost MW radiometer; Tech-demonstration
	ISS-TEMPEST-D	NASA	2018	89–192	Precess.	825	n/a		Mm wave radiometer; Tech-demonstration
Lidar	Aeolus	ESA	2018	355 nm	6:00 (D)	87	NO	87(H) 1–2(V)	Doppler Lidar Wind profiler. Recently ended (July 2023)

(*continued on next page*)

(*continued*)

Type	Sat/sensor	Agency	Launch	Freq (GHz)	Orbit	Swath Width (km)	All-weather winds	Wind Res. (km)	Comments
VIS/IR Sounders (Polar orbiters)	AIRS (Aqua)	NASA	2002	0.41–15 mm	13:30 (A)	1650	n/a		IR sounder T/q sounder
	CrIS 1.NOAA-20 2.SNPP	NOAA	2017 2011	3.9–15 mm	13:25 (A) 13:25 (A)	2200	n/a		IR sounder T/q/WV
	HIRS/4 1.MetOp-B 2.NOAA18 3.NOAA19	NOAA	2012 2005 2009	0.69–15 mm	9:30 (D) 8:05 (D) 7:30 (D)	2200	n/a		VIS/IR T/q/WV sounder
	IASI 1.MetOp-B 2. MetOp-C	CNES	2021 2018	3–15.5 mm	9:30 (D)	2130	n/a		IR Interferometric Sounder T/q/WV
	HIRAS 1.FY-3D 2.FY-3E	CMA	2018	3.9–15.4 mm	13:30 (A) 5:40 (A)	2400	n/a		Hyperspectral IR sounder
	VIIRS 1.NOAA-20 2.SNPP	NASA	2017 2011	0.4–12 mm	13:25 (A) 13:25 (A)	3000	n/a		VIS/IR Imager, Day/night SST, clouds, integrated WV
	AVHRR/3 1.MetOp-B 2.NOAA18 3.NOAA19	NOAA	2012 2005 2009	0.58–12.5 mm	9:30 (D) 8:05 (D) 7:30 (D)	2900	n/a		High resolution Vis/IR radiometer SST, clouds

Appendix C. Data Distribution Links

The major TC Satellite Data/Imaging distribution links are:

1) US Navy FNMOC: https://www.fnmoc.navy.mil/tcweb/cgi-bin/tc_home.cgi.

2) US Navy ATCF: https://www.nrlmry.navy.mil/atcf_web/

3) CIMSS, University of Wisconsin: https://tropic.ssec.wisc.edu/

Additional sensor-specific data distribution links are.

SAR

IFREMER: https://cyclobs.ifremer.fr/app/tropical.

The IFREMER web page provides SAR Data (operational RadarSat2 and Sentinel 1A; archived 1B) and imagery for recent and archived storms. It displays SMAP/SMOS overpasses too. There is ample SAR validation statistics which helps familiarizing with the data accuracy. SAR data are available in Near Real Time (NRT) with latency of about 2.5–5 h.

NOAA/NESDIS/STAR SAROPS: https://www.star.nesdis.noaa.gov/socd/mecb/sar/AKDEMO_products/APL_winds/tropical/

The NOAA/NESDIS/STAR SAROPS web page includes data for operational RadarSat2, and RCM 1,2,3, and Sentinel 1A, and archived 1B. It provides ample information that is critical to helping the analyst make sense of the SAR data including, the distribution graphs, Fix data and the averaging information. Fix data is also sent in ATCF via NRL. Usually, the data is available on the NOAA STAR webpage a bit after it is sent in ATCF due to the extra processing and product generation they do that NRL does not.

RadarSat-2, Earth Observation Data Management System, Government of Canada

https://eodms-sgdot.nrcan-rncan.gc.ca/index-en.html.

The Canadian web page provides raw SAR data for the RCM missions.

SMAP

REMSS TC fixes/images: https://www.remss.com/tropical-cyclones/tc-winds/

REMSS Global *gridded winds, L3*: https://www.remss.com/missions/smap/

The REMSS TC Fixes are also distributed via FNMOC and NRL ATCF. NRT Latency for the gridded data is 2–3 h; for the TC fixes is 2–6 h, as TC-fix processing waits for the availability of an estimated storm center from IBTracks. This could be shortened in the future if an automated storm detection center is implemented. The daily L3 data (NetCDF file) are gridded on a 25 × 25 km ascending/descending grid but actual resolution is about 40 km; the daily file is updated every time a new orbit within the day is processed.

NASA JPL global winds: https://podaac.jpl.nasa.gov/dataset/SMAP_JPL_L2B_NRT_SSS_CAP_V5?ids=&values=&search=smap%20wind&provider=PODAAC.

Comments: the NASA JPL SMAP winds have an NRT product which includes winds and salinity. This product has a latency of 6 h. They are distributed as 25 km swath grid (L2B) with an approximate spatial resolution of 60 km. NetCDF files.

SMOS

IFREMER: www.smosstorm.org.

Three products available in NRT (latency 6 h): Wind radii fixes (WRF), gridded swath winds (L2), and gridded daily (L3, asc/desc), on a 25 km swath grid (L2B) with an approximate spatial resolution of 60 km.

SCATTEROMETERS:

KNMI OSI SAF: https://scatterometer.knmi.nl/osisaf/

Several scatterometer data are available from KNMI: ASCAT-B/C, HY-2B/C, CFOSat.

NOAA/NESDIS/STAR: https://manati.star.nesdis.noaa.gov/

ASCAT-B/C operational data processed in NRT, latency 2.5–3.5 h; distribution via the ATCF/FNMOC TCWeb is a little faster, 1.5–2.5 h.

REMSS ASCAT: https://www.remss.com/ascat.

This is a research-oriented product, with high winds cross-calibrated to the other REMSS satellite winds, part of the REMSS ocean surface winds Climate Data Record. At this time, it is not processed in NRT, and the latency is of the order of 7–10 days.

Microwave Imagers/Sounders

In addition to the major data distribution centers, MW imagers processed in NRT are available at**:**

REMSS MW missions: https://www.remss.com/

The following imagers/sounders are processed/distributed in NRT: SSMIS, AMSR2, GMI, AMSU.

REMSS AMSR2 TC-winds: https://www.remss.com/tropical-cyclones/tc-winds/

Recently, REMSS started processing TC-fixes (wind radii) and TC-winds from AMSR2. Note that this is a TC-specific product, specifically developed for tropical storm conditions. This is different from the global all-weather AMSR2 winds available at https://www.remss.com/missions/amsr/. The AMSR2 TC-winds are consistent with REMSS SMAP TC-winds, available at the same link.

NOAA AMSR2 all-weather winds: https://manati.star.nesdis.noaa.gov/datasets/GCOM2Data.php.

Aeolus

Data from the Aeolus wind profiler are available at: https://earth.esa.int/eogateway/missions/aeolus/data.

CYGNSS

Different products for the CYGNSS mission are available here (no NRT):

https://podaac.jpl.nasa.gov/CYGNSS.

Daily images of the NOAA CYGNSS winds are available on the following web-browser (2–3 days latency).

https://manati.star.nesdis.noaa.gov/datasets/CYGNSSData.php.

ProxyVis

Information on ProxyVis and data access is available here: https://rammb2.cira.colostate.edu/research/goes-r-research/proxyvis/

Appendix D. Sensors used in operations

Black checkmarks refer to sensors routinely used in operations. Red checkmarks refer to sensors currently under evaluation, but not used in operations.

		NHC	JTWC	BoM	PAGASA	IMD	La Reunion	JMA	KMA	CMA	CHC	UKMO	ECMWF
SAR	Sentinel 1A	Y	Y	Y	Y	Y	Y				Y		
	RadarSat2, RCM	Y	Y	Y	Y		Y				Y		
	GF-3									Y			
L-band Winds	SMAP		Y	Y			Y						
	SMOS		Y	Y			Y						
X/C band Radiometers	AMSR2 all-weather or TC winds		Y	Y				Y					
	AMSR2 Radiance	Y	Y	Y	Y	Y	Y	Y	Y	Y			Y
Scatterometers	ASCAT-	Y	Y	Y	Y	Y	Y	Y	Y			Y	Y
	HY-2B/2C		Y	Y	Y		Y	Y	Y	Y			
	CFOSat		Y	Y	Y								
	WindRad									Y			

(*continued on next page*)

(*continued*)

		NHC	JTWC	BoM	PAGASA	IMD	La Reunion	JMA	KMA	CMA	CHC	UKMO	ECMWF
MW and IR Imagers/Sounders	SSMIS	Y	Y	Y	Y	Y	Y	Y	Y			Y	Y
	GPM (GMI/DPR)	Y	Y	Y	Y	Y	Y	Y	Y				Y
	ATMS (NOAA-20, NPP)	Y	Y	Y	Y		Y	Y	Y	Y		Y	Y
	AMSU (MetOp-B/C/ NOAA)	Y	Y		Y			Y		Y		Y	Y
	AIRS (Aqua)												
	CrIS (NOAA-20,NPP)							Y		Y		Y	
	ATOVS (NOAA-15/ 18/19)											Y	Y
	IASI (MetOp-B/C)							Y		Y		Y	
	MHS		Y	Y				Y	Y	Y			Y
	MWHS/MHTS (FY-3C/E)							Y		Y		Y	Y
	MWRI (FY-3D)									Y		Y	
	HIRAS									Y			
Small Sats	TROPICS		Y										
	COWVR		Y										
	TEMPEST-D		Y										
Lidar	Aeolus									Y		Y	Y
GNSS-RO	MetOp-B/C							Y				Y	Y
	IGOR							Y					Y
	FY-3C/D									Y		Y	
	KompSat-5											Y	Y
	SPIRE											Y	Y
	PAZ											Y	
	Sentinel-6A											Y	Y
VIS/IR Sounders (LEO)	AIRS (Aqua)												Y
	CrIS (NOAA-20,NPP)							Y				Y	Y
	HIRS/4(Metop-B/18/ 19)											Y	
	IASI (MetOp-B/C)							Y				Y	Y
	HIRAS									Y			
Geostationary (VIS/IR)	GOES 16, 17, 18	Y	Y					Y				Y	Y
	MeteoSat-8/9/11	Y	Y			Y		Y				Y	Y
	EW-SG (GOES 13)		Y										
	Himawari-8		Y	Y	Y			Y	Y			Y	Y
	FY-4A/B									Y			
	MSG2						Y						
	INSAT 3D, 3DR					Y							
	GK-2A								Y				
	Seviri												
	GLM	Y											

References

Alsweiss, S., Sapp, J., Jelenak, Z., Chang, P., 2021. An operational all-weather wind speed from AMSR2. In: 2021 IEEE International Geoscience and Remote Sensing Symposium IGARSS. Presented at the IGARSS 2021 - 2021 IEEE International Geoscience and Remote Sensing Symposium. IEEE, Brussels, Belgium, pp. 7334–7337. https://doi.org/10.1109/IGARSS47720.2021.9553710.

Bessho, K., Date, K., Hayashi, M., Ikeda, A., Imai, T., Inoue, H., Kumagai, Y., Miyakawa, T., Murata, H., Ohno, T., Okuyama, A., Oyama, R., Sasaki, Y., Shimazu, Y., Shimoji, K., Sumida, Y., Suzuki, M., Taniguchi, H., Tsuchiyama, H., Uesawa, D., Yokota, H., Yoshida, R., 2016. An introduction to Himawari-8/9; Japan's new-generation geostationary meteorological satellites. J. Meteorol. Soc. Jpn. 94, 151–183. https://doi.org/10.2151/jmsj.2016-009.

Blackwell, W.J., Braun, S., Bennartz, R., Velden, C., DeMaria, M., Atlas, R., Dunion, J., Marks, F., Rogers, R., Annane, B., Leslie, R.V., 2018. An overview of the TROPICS NASA earth venture mission. Q. J. R. Meteorol. Soc. 144, 16–26. https://doi.org/10.1002/qj.3290.

Blackwell, W.J., Cunningham, A., Donnelly, S., Leslie, R.V., Zorn, N., 2022. The NASA tropics mission as a pathfinder for future LEO microwave sounders. In: IGARSS 2022 - 2022 IEEE International Geoscience and Remote Sensing Symposium. Presented at the IGARSS 2022 - 2022 IEEE International Geoscience and Remote Sensing Symposium. IEEE, Kuala Lumpur, Malaysia, pp. 4873–4874. https://doi.org/10.1109/IGARSS46834.2022.9884090.

Brown, S., Berg, W., Gaier, T., Kangaslahti, P.P., Kitiyakara, A., Lim, B., Padmanabhan, S., Reising, S., Venkatachalam, C., 2019. New small satellite passive microwave radiometer technology for future constellation missions (Conference Presentation). In: Neeck, S.P., Kimura, T., Martimort, P. (Eds.), Sensors, Systems, and Next-Generation Satellites XXIII. Presented at the Sensors, Systems, and Next-Generation Satellites XXIII. SPIE, Strasbourg, France, p. 17. https://doi.org/10.1117/12.2533341.

Brown, S.T., Misra, S., Kitiyakara, A., Morris, M., 2021. Compact Ocean wind vector radiometer on ISS mission status. Presentation available at. https://trs.jpl.nasa.gov/bitstream/handle/2014/54531/CL%2321-0870.pdf?sequence=1.

Carreno-Luengo, H., Crespo, J.A., Akbar, R., Bringer, A., Warnock, A., Morris, M., Ruf, C., 2021. The CYGNSS mission: on-going science team investigations. Remote Sensing 13, 1814. https://doi.org/10.3390/rs13091814.

Chen, Z., Yu, X., Chen, G., Zhou, J., 2018. Cyclone intensity estimation using multispectral imagery from the FY-4 satellite. In: 2018 International Conference on Audio, Language and Image Processing (ICALIP). Presented at the 2018 International Conference on Audio, Language and Image Processing (ICALIP). IEEE, Shanghai, China, pp. 46–51. https://doi.org/10.1109/ICALIP.2018.8455603.

Chirokova, G., Knaff, J.A., Brennan, M.J., DeMaria, R.T., Bozeman, M., Stevenson, S.N., Beven, J.L., Blake, E.S., Brammer, A., Darlow, J.W., DeMaria, M., Miller, S.D., Slocum, C.J., Molenar, D., Hillger, D.W., 2023. ProxyVis – a Proxy for Nighttime Visible Imagery Applicable to Geostationary Satellite Observations. Weather and Forecasting. https://doi.org/10.1175/WAF-D-23-0038.1.

Duong, Q.-P., Langlade, S., Payan, C., Husson, R., Mouche, A., Malardel, S., 2021. C-band SAR winds for tropical cyclone monitoring and forecast in the south-west Indian Ocean. Atmosphere 12, 576. https://doi.org/10.3390/atmos12050576.

Dvorak, V.F., 1975. Tropical cyclone intensity analysis and forecasting from satellite imagery. Mon. Wea. Rev. 103, 420–430. https://doi.org/10.1175/1520-0493(1975)103<0420:TCIAAF>2.0.CO;2.

Fang, H., Perrie, W., Fan, G., Li, Z., Cai, J., He, Y., Yang, J., Xie, T., Zhu, X., 2022. High-resolution sea surface wind speeds of Super Typhoon Lekima (2019) retrieved by Gaofen-3 SAR. Front. Earth Sci. 16, 90–98. https://doi.org/10.1007/s11707-021-0887-8.

Garrett, K., Liu, H., Ide, K., Hoffman, R.N., Lukens, K.E., 2022. Optimization and impact assessment of Aeolus HLOS wind assimilation in NOAA 's global forecast system. Quart J. R. Meteoro Soc. 148, 2703–2716. https://doi.org/10.1002/qj.4331.

Geer, Baordo, Boardman, English, 2014. All-sky Assimilation of Microwave Humidity Sounders. ECMWF Tech. Memo. No. 741).

Goodman, S.J., 2020. GOES-R series introduction. In: The GOES-R Series. Elsevier, pp. 1–3. https://doi.org/10.1016/B978-0-12-814327-8.00001-9.

Hart, R.E., 2003. A cyclone phase space derived from thermal wind and thermal asymmetry. Mon. Wea. Rev. 131, 585–616. https://doi.org/10.1175/1520-0493(2003)131<0585:ACPSDF>2.0.CO;2.

He, Y., 2020. Round-trip Airborne Flat-Floating Sounding System (RTAFSS) Data-2. https://doi.org/10.4121/UUID:868C025A-1B30-42A8-B722-E6CB66B0AE22.

Holbach, H.M., Bousquet, O., Bucci, L., Chang, P., Cione, J., Ditchek, S., Doyle, J., Duvel, J.-P., Elston, J., Goni, G., Hon, K.K., Ito, K., Jelenak, Z., Lei, X., Lumpkin, R., McMahon, C.R., Reason, C., Sanabia, E., Shay, L.K., Sippel, J.A., Sushko, A., Tang, J., Tsuboki, K., Yamada, H., Zawislak, J., Zhang, J.A., 2023. Recent advancements in aircraft and in situ observations of tropical cyclones. Trop. Cycl. Res. Rev. 12, 81–99. https://doi.org/10.1016/j.tcrr.2023.06.001.

Holmlund, K., Grandell, J., Schmetz, J., Stuhlmann, R., Bojkov, B., Munro, R., Lekouara, M., Coppens, D., Viticchie, B., August, T., Theodore, B., Watts, P., Dobber, M., Fowler, G., Bojinski, S., Schmid, A., Salonen, K., Tjemkes, S., Aminou, D., Blythe, P., 2021. Meteosat third generation (MTG): continuation and innovation of observations from geostationary orbit. Bull. Am. Meteorol. Soc. 102, E990–E1015. https://doi.org/10.1175/BAMS-D-19-0304.1.

Howell, B., Egan, S., Fine, C., 2022. Application of microwave space-based environmental monitoring (SBEM) data for operational tropical cyclone intensity estimation at the joint typhoon warning center. Bull. Am. Meteorol. Soc. 103, E2315–E2322. https://doi.org/10.1175/BAMS-D-21-0180.1.

Isoguchi, O., Tadono, T., Ohki, M., Shimada, U., Yamaguchi, M., Hayashi, M., Yanase, W., 2021. Hurricane Ocean surface wind retrieval from ALOS-2 PALSAR-2 cross-polarized measurements. In: 2021 IEEE International Geoscience and Remote Sensing Symposium IGARSS. Presented at the IGARSS 2021 - 2021 IEEE International Geoscience and Remote Sensing Symposium. IEEE, Brussels, Belgium, pp. 7291–7294. https://doi.org/10.1109/IGARSS47720.2021.9554411.

Jackson, C., Ruff, T., Knaff, J., Mouche, A., Sampson, C., 2021. Chasing cyclones from space. Eos 102. https://doi.org/10.1029/2021EO159148.

Kazumori, Kadowaki, 2017. Development of an all-sky assimilation of microwave imager and sounder radiances for the Japan Meteorological Agency global numerical weather prediction system. Proc. 21st Int. TOVS Study Conf. 20, 2017. Available at. https://cimss.ssec.wisc.edu/itwg/itsc/itsc21/proceedings/5.04_kazumori.pdf.

Kim, D., Gu, M., Oh, T.-H., Kim, E.-K., Yang, H.-J., 2021. Introduction of the advanced meteorological imager of Geo-Kompsat-2a: in-orbit tests and performance validation. Remote Sensing 13, 1303. https://doi.org/10.3390/rs13071303.

Knaff, J.A., Sampson, C.R., Kucas, M.E., Slocum, C.J., Brennan, M.J., Meissner, T., Ricciardulli, L., Mouche, A., Reul, N., Morris, M., Chirokova, G., Caroff, P., 2021. Estimating tropical cyclone surface winds: current status, emerging technologies, historical evolution, and a look to the future. Trop. Cycl. Res. Rev. 10, 125–150. https://doi.org/10.1016/j.tcrr.2021.09.002.

Li, X.-M., Zhang, T., Huang, B., Jia, T., 2018. Capabilities of Chinese Gaofen-3 synthetic aperture radar in selected topics for coastal and ocean observations. Remote Sensing 10, 1929. https://doi.org/10.3390/rs10121929.

Li, Z., Stoffelen, A., Verhoef, A., 2019. A generalized simulation capability for rotating- beam scatterometers. Atmos. Meas. Tech. 12, 3573–3594. https://doi.org/10.5194/amt-12-3573-2019.

Manaster, A., Ricciardulli, L., Meissner, T., 2021. Tropical cyclone winds from WindSat, AMSR2, and SMAP: comparison with the HWRF model. Remote Sensing 13, 2347. https://doi.org/10.3390/rs13122347.

Marinescu, P.J., Cucurull, L., Apodaca, K., Bucci, L., Genkova, I., 2022. The characterization and impact of Aeolus wind profile observations in NOAA 's regional tropical cyclone model (HWRF). Quart J. R. Meteoro Soc. qj 4370. https://doi.org/10.1002/qj.4370.

Martin, S., 2014. An Introduction to Ocean Remote Sensing, second ed. Cambridge University Press. https://doi.org/10.1017/CBO9781139094368.

Mayers, D.R., Ruf, C.S., Warnock, A.M., 2023. CYGNSS storm-centric tropical cyclone gridded wind speed product. J. Appl. Meteorology Climatology 62, 329–339. https://doi.org/10.1175/JAMC-D-22-0054.1.

Meissner, T., Ricciardulli, L., Manaster, A., 2021. Tropical cyclone wind speeds from WindSat, AMSR and SMAP: algorithm development and testing. Remote Sensing 13, 1641. https://doi.org/10.3390/rs13091641.

Meissner, T., Ricciardulli, L., Wentz, F.J., 2017. Capability of the SMAP mission to measure ocean surface winds in storms. Bull. Am. Meteorol. Soc. 98, 1660–1677. https://doi.org/10.1175/BAMS-D-16-0052.1.

Mouche, A., Chapron, B., Knaff, J., Zhao, Y., Zhang, B., Combot, C., 2019. Copolarized and cross-polarized SAR measurements for high-resolution description of major hurricane wind structures: application to Irma category 5 hurricane. J. Geophys. Res. Oceans 124, 3905–3922. https://doi.org/10.1029/2019JC015056.

Mouche, A.A., Chapron, B., Zhang, B., Husson, R., 2017. Combined Co- and cross-polarized SAR measurements under extreme wind conditions. IEEE Trans. Geosci. Remote Sensing 55, 6746–6755. https://doi.org/10.1109/TGRS.2017.2732508.

Ni, W., Stoffelen, A., Ren, K., 2022. Hurricane eye morphology extraction from SAR images by texture analysis. Front. Earth Sci. 16, 190–205. https://doi.org/10.1007/s11707-021-0886-9.

Nonaka, K., Nishimura, S., Igarashi, Y., 2019. Utilization of Estimated Sea Surface WindData Based on Himawari-8/9 Low-Level AMVs for Tropical Cyclone Analysis. RSMC Tokyo Typhoon Center Technical Review 21. Available at:https://www.jma.go.jp/jma/jma-eng/jma-center/rsmc-hp-pub-eg/techrev/text21-3.pdf.

Otsuka, M., Seko, H., Shimoji, K., Yamashita, K., 2018. Characteristics of Himawari-8 rapid scan atmospheric motion vectors utilized in mesoscale data assimilation. J. Meteorol. Soc. Jpn. 96B, 111–131. https://doi.org/10.2151/jmsj.2018-034.

Polverari, F., Portabella, M., Lin, W., Sapp, J.W., Stoffelen, A., Jelenak, Z., Chang, P.S., 2022. On high and extreme wind calibration using ASCAT. IEEE Trans. Geosci. Remote Sensing 60, 1–10. https://doi.org/10.1109/TGRS.2021.3079898.

Portabella, M., Stoffelen, A., Lin, W., Turiel, A., Verhoef, A., Verspeek, J., Ballabrera-Poy, J., 2012. Rain effects on ASCAT-retrieved winds: toward an improved quality control. IEEE Trans. Geosci. Remote Sensing 50, 2495–2506. https://doi.org/10.1109/TGRS.2012.2185933.

Radhakrishnan, C., Chandrasekar, V., Reising, S.C., Berg, W., Brown, S.T., Tanelli, S., Sy, O.O., Sacco, G.F., 2022. Cross validation of TEMPEST-D and RainCube observations over precipitation systems. IEEE J. Sel. Top. Appl. Earth Observations Remote Sensing 15, 7826–7838. https://doi.org/10.1109/JSTARS.2022.3199402.

Reising, S.C., Gaier, T.C., Padmanabhan, S., Lim, B.H., Heneghan, C., Kummerow, C.D., Berg, W., Chandrasekar, V., Radhakrishnan, C., Brown, S.T., Carvo, J., Pallas, M., 2018. An earth venture in-space technology demonstration mission for temporal experiment for storms and tropical systems (tempest). In: IGARSS 2018 - 2018 IEEE International Geoscience and Remote Sensing Symposium. Presented at the IGARSS 2018 - 2018 IEEE International Geoscience and Remote Sensing Symposium. IEEE, Valencia, pp. 6301–6303. https://doi.org/10.1109/IGARSS.2018.8517330.

Rennie, M.P., Isaksen, L., Weiler, F., Kloe, J., Kanitz, T., Reitebuch, O., 2021. The impact of Aeolus wind retrievals on ECMWF global weather forecasts. Q. J. R. Meteorol. Soc. 147, 3555–3586. https://doi.org/10.1002/qj.4142.

Reul, N., Chapron, B., Zabolotskikh, E., Donlon, C., Quilfen, Y., Guimbard, S., Piolle, J.F., 2016. A revised L-band radio-brightness sensitivity to extreme winds under Tropical Cyclones: the five year SMOS-storm database. Remote Sensing Environ. 180, 274–291. https://doi.org/10.1016/j.rse.2016.03.011.

Reul, N., Tenerelli, J., Chapron, B., Vandemark, D., Quilfen, Y., Kerr, Y., 2012. SMOS satellite L-band radiometer: A new capability for ocean surface remote sensing in hurricanes: SMOS L-BAND RADIOMETER AND HIGH WINDS. J. Geophys. Res. 117. https://doi.org/10.1029/2011JC007474 n/a-n/a.

Ricciardulli, L., Manaster, A., 2021. Intercalibration of ASCAT scatterometer winds from MetOp-A, -B, and -C, for a stable climate data record. Remote Sensing 13, 3678. https://doi.org/10.3390/rs13183678.

Ricciardulli, L., Mears, C., Manaster, A., Meissner, T., 2021. Assessment of CYGNSS wind speed retrievals in tropical cyclones. Remote Sensing 13, 5110. https://doi.org/10.3390/rs13245110.

Ricciardulli, L., Wentz, F.J., 2015. A scatterometer geophysical model function for climate-quality winds: QuikSCAT ku-2011. J. Atmos. Ocean. Technol. 32, 1829–1846. https://doi.org/10.1175/JTECH-D-15-0008.1.

Ruf, C., Asharaf, S., Balasubramaniam, R., Gleason, S., Lang, T., McKague, D., Twigg, D., Waliser, D., 2019. In-orbit performance of the constellation of CYGNSS hurricane satellites. Bull. Am. Meteorol. Soc. 100, 2009–2023. https://doi.org/10.1175/BAMS-D-18-0337.1.

Ruf, C.S., Chew, C., Lang, T., Morris, M.G., Nave, K., Ridley, A., Balasubramaniam, R., 2018. A new paradigm in earth environmental monitoring with the CYGNSS small satellite constellation. Sci. Rep. 8, 8782. https://doi.org/10.1038/s41598-018-27127-4.

Ruf, C.S., Gleason, S., McKague, D.S., 2019. Assessment of CYGNSS wind speed retrieval uncertainty. IEEE J. Sel. Top. Appl. Earth Observations Remote Sensing 12, 87–97. https://doi.org/10.1109/JSTARS.2018.2825948.

Said, F., Jelenak, Z., Park, J., Chang, P.S., 2021. The NOAA track-wise wind retrieval algorithm and product assessment for CyGNSS. IEEE Trans. Geosci. Remote Sensing 1–24. https://doi.org/10.1109/TGRS.2021.3087426.

Said, F., Jelenak, Z., Park, J., Soisuvarn, S., Chang, P.S., 2019. A 'track-wise' wind retrieval algorithm for the CYGNSS mission. In: IGARSS 2019 - 2019 IEEE International Geoscience and Remote Sensing Symposium. Presented at the IGARSS 2019 - 2019 IEEE International Geoscience and Remote Sensing Symposium, pp. 8711–8714. https://doi.org/10.1109/IGARSS.2019.8898099.

Sampson, C.R., Schrader, A.J., 2000. The automated tropical cyclone forecasting system (version 3.2). Bull. Amer. Meteorol. Soc. 81, 1231–1240. https://doi.org/10.1175/1520-0477(2000)081<1231:TATCFS>2.3.CO;2.

Schmetz, J., Pili, P., Tjemkes, S., Just, D., Kerkmann, J., Rota, S., Ratier, A., 2002. Supplement to an introduction to Meteosat second generation (MSG): SEVIRI CALIBRATION. Bull. Amer. Meteorol. Soc. 83, 992. https://doi.org/10.1175/BAMS-83-7-Schmetz-2, 992.

Shibata, A., 2006. A wind speed retrieval algorithm by combining 6 and 10 GHz data from Advanced Microwave Scanning Radiometer: wind speed inside hurricanes. J. Oceanogr. 62, 351–359. https://doi.org/10.1007/s10872-006-0060-8.

Soisuvarn, S., Jelenak, Z., Chang, P.S., Alsweiss, S.O., Zhu, Q., 2013. CMOD5.H—a high wind geophysical model function for C-band vertically polarized satellite scatterometer measurements. IEEE Trans. Geosci. Remote Sensing 51, 3744–3760. https://doi.org/10.1109/TGRS.2012.2219871.

Stiles, B.W., Yueh, S.H., 2002. Impact of rain on spaceborne Ku-band wind scatterometer data. IEEE Trans. Geosci. Remote Sensing 40, 1973–1983. https://doi.org/10.1109/TGRS.2002.803846.

Stoffelen, A., 1998. Toward the true near-surface wind speed: error modeling and calibration using triple collocation. J. Geophys. Res. 103, 7755–7766. https://doi.org/10.1029/97JC03180.

Stoffelen, A., Aaboe, S., Calvet, J.-C., Cotton, J., De Chiara, G., Saldana, J.F., Mouche, A.A., Portabella, M., Scipal, K., Wagner, W., 2017a. Scientific developments and the EPS-SG scatterometer. IEEE J. Sel. Top. Appl. Earth Observations Remote Sensing 10, 2086–2097. https://doi.org/10.1109/JSTARS.2017.2696424.

Stoffelen, A., Benedetti, A., Borde, R., Dabas, A., Flamant, P., Forsythe, M., Hardesty, M., Isaksen, L., Källén, E., Körnich, H., Lee, T., Reitebuch, O., Rennie, M., Riishøjgaard, L.-P., Schyberg, H., Straume, A.G., Vaughan, M., 2020. Wind profile satellite observation requirements and capabilities. Bull. Am. Meteorol. Soc. 101, E2005–E2021. https://doi.org/10.1175/BAMS-D-18-0202.1.

Stoffelen, A., Verspeek, J.A., Vogelzang, J., Verhoef, A., 2017b. The CMOD7 geophysical model function for ASCAT and ERS wind retrievals. IEEE J. Sel. Top. Appl. Earth Observations Remote Sensing 10, 2123–2134. https://doi.org/10.1109/JSTARS.2017.2681806.

Velden, C., Harper, B., Wells, F., Beven, J.L., Zehr, R., Olander, T., Mayfield, M., Guard, C."C.H.I.P., Lander, M., Edson, R., Avila, L., Burton, A., Turk, M., Kikuchi, A., Christian, A., Caroff, P., McCrone, P., 2006. The Dvorak tropical cyclone intensity estimation technique: a satellite-based method that has endured for over 30 years. Bull. Amer. Meteorol. Soc. 87, 1195–1210. https://doi.org/10.1175/BAMS-87-9-1195.

Velden, C.S., Herndon, D., 2020. A consensus approach for estimating tropical cyclone intensity from meteorological satellites: SATCON. Weather Forecast. 35, 1645–1662. https://doi.org/10.1175/WAF-D-20-0015.1.

Wang, H., Zhu, J., Lin, M., Zhang, Y., Chang, Y., 2020. Evaluating Chinese HY-2B HSCAT Ocean Wind products using Buoys and other scatterometers. IEEE Geosci. Remote Sensing Lett. 17, 923–927. https://doi.org/10.1109/LGRS.2019.2940384.

Wang, L., Wan, B., Zhou, S., Sun, H., Gao, Z., 2023. Forecasting tropical cyclone tracks in the northwestern Pacific based on a deep-learning model. Geosci. Model Dev. (GMD) 16, 2167–2179. https://doi.org/10.5194/gmd-16-2167-2023.

Wang, Z., Zou, J., Stoffelen, A., Lin, W., Verhoef, A., Li, X., He, Y., Zhang, Y., Lin, M., 2021. Scatterometer Sea surface wind product validation for HY-2C. IEEE J. Sel. Top. Appl. Earth Observations Remote Sensing 14, 6156–6164. https://doi.org/10.1109/JSTARS.2021.3087742.

Wentz, F.J., Ricciardulli, L., Rodriguez, E., Stiles, B.W., Bourassa, M.A., Long, D.G., Hoffman, R.N., Stoffelen, A., Verhoef, A., O'Neill, L.W., Farrar, J.T., Vandemark, D., Fore, A.G., Hristova-Veleva, S.M., Turk, F.J., Gaston, R., Tyler, D., 2017. Evaluating and extending the Ocean Wind climate data record. IEEE J. Selected Top. Appl. Earth Observations Remote Sensing 10, 2165–2185. https://doi.org/10.1109/JSTARS.2016.2643641.

WMO, 2022. 10th International Workshop on Tropical Cyclones (IWTC-10). WMO, Bali, Indonesia. Available at. https://community.wmo.int/en/iwtc-10-reports.

WMO, 2018. Ninth International Workshop on Tropical Cyclones (IWTC-9), (WWRP 2020-2). WMO, Hawaii. Available at. https://library.wmo.int/doc_num.php?explnum_id=11006.

WMO, IWSATC-3, 2022. Third International Workshop on Satellite Analysis of Tropical Cyclones (IWSATC-3). WMO Report 2022. Prepared by J. Courtney and D. Herndon. Available at. https://library.wmo.int/doc_num.php?explnum_id=11126.WMO.

Xu, X., Stoffelen, A., 2020. Improved rain screening for Ku-band wind scatterometry. IEEE Trans. Geosci. Remote Sensing 58, 2494–2503. https://doi.org/10.1109/TGRS.2019.2951726.

Zhang, B., Perrie, W., 2012. Cross-polarized synthetic aperture radar: a new potential measurement technique for hurricanes. Bull. Am. Meteorol. Soc. 93, 531–541. https://doi.org/10.1175/BAMS-D-11-00001.1.

Zhang, P., Hu, X., Lu, Q., Zhu, A., Lin, M., Sun, L., Chen, L., Xu, N., 2022. FY-3E: the first operational meteorological satellite mission in an early morning orbit. Adv. Atmos. Sci. 39, 1–8. https://doi.org/10.1007/s00376-021-1304-7.

Zhao, Y., Mouche, A.A., Chapron, B., Reul, N., 2018. Direct comparison between active C-band radar and passive L-band radiometer measurements: extreme event cases. IEEE Geosci. Remote Sensing Lett. 15, 897–901. https://doi.org/10.1109/LGRS.2018.2811712.

Zou, X., 2021. Studies of FY-3 observations over the past 10 Years: a review. Remote Sensing 13, 673. https://doi.org/10.3390/rs13040673.